MINISTRY OF SUPPLY

AERONAUTICAL RESEARCH COUNCIL
REPORTS AND MEMORANDA

Low-Speed Experiments on the Wake Characteristics of Flat Plates normal to an Air Stream

By

R. FAIL, J. A. LAWFORD and R. C. W. EYRE

LONDON: HER MAJESTY'S STATIONERY OFFICE

1959

PRICE 10s. 6d. NET

Low-Speed Experiments on the Wake Characteristics of Flat Plates normal to an Air Stream

By

R. Fail, J. A. Lawford and R. C. W. Eyre

Communicated by the Director-General of Scientific Research (Air),
Ministry of Supply

Reports and Memoranda No. 3120*

June, 1957

Summary.—Experiments on isolated flat plates perpendicular to the wind are described.

It is shown that the effects of aspect ratio on drag, base pressure and flow pattern are small up to $A = 10$. All of these rectangular plates shed turbulent eddies at particular frequencies; generally there are two shedding frequencies for each plate, one associated with the smaller dimension of the plate, and a lower frequency associated with the larger dimension.

Large changes in the shape of low-aspect-ratio plates have very small effects on the aerodynamic characteristics but perforating the plate can eliminate the regular shedding of eddies and reduce the random low-frequency velocity fluctuations.

---

1. *Introduction.*—Some preliminary experiments on flat plates with particular reference to their use as air brakes have been described in Ref. 1. The present paper deals with the basic aerodynamic characteristics of flat plates normal to an air stream, and includes examination of the effects of varying the shape of the plate.

The main feature of the flow around an unperforated plate is a closed 'bubble' behind the plate. This type of flow is illustrated in Fig. 1, which refers to a circular plate and is based on the detailed measurements given in the body of the present report. Fig. 1a shows the mean streamlines behind the plate. The closed part of the streamline $\psi = 0$, behind the plate, is referred to as the 'bubble boundary'. Within the bubble there is a ring of circulatory flow and associated variations in static pressure (Fig. 1c). The 'wake boundary' (outside which there is no loss of total head) lies outside the bubble boundary (Fig. 1b) but is of similar shape to the bubble boundary up to about the mid-length of the bubble. Over the rear surface of the plate and along the wake boundary, up to about the mid-length of the bubble, the static-pressure coefficient is constant and equal to -0.42† (Fig. 1c). The corresponding velocity is about $1.2U_0$†. Behind the mid-length of the bubble, the wake spreads and a pressure recovery occurs (Fig. 1c).

The flow is unsteady and velocity fluctuations occur behind the plate both at random and at particular frequencies. The latter fluctuations are due to a regular shedding of turbulent eddies.

The formation of the bubble behind the plate and the associated regular shedding can be prevented by perforating the plate; work on this is described in Ref. 2.

Some of the data already presented in Ref. 1 are repeated in the present paper, sometimes with slight changes in the values used. This is because a mean blockage correction was used in Ref. 1, whereas this is now known to vary with the base-pressure coefficient as shown in Ref. 3.

2. *Description of Tests.*—The experiments can be divided into two groups; in all cases the plates were perpendicular to the wind:

(1) Tests on a series of rectangular plates, of area 25 sq in., having aspect ratios of 1, 2, 5, 10 and 20; some measurements are included which were made on a plate of aspect ratio 2·15 and area 27 sq in. It is noted that since the plates were always normal to the air stream, a plate having an aspect ratio A has equally an aspect ratio $1/A$. Tests were also made on a plate of chord 1·24 in. which spanned the 3-ft dimension of the tunnel.

(2) Tests on a series of plates of different shapes. These included an equilateral triangle and a circle, both of area 25 sq in. and a circular plate with tabs having a total area of 18·6 sq in. (Fig. 2).

In general the following tests were made on each plate:

(*a*) The drag of the plate

(*b*) The base pressure on the plate

(*c*) An investigation of the mean flow pattern behind the plate, using pitot-static tubes

(*d*) An investigation of the velocity fluctuation behind the plate, using a hot wire normal to the free stream.

The experiments were made in the 4 ft × 3 ft Wind Tunnel at a speed of 140 ft/sec. The plates were mounted on the upstream end of a rod about 3 ft long and 0·5-in. diameter on the axis of the tunnel. The downstream end of the rod was supported by struts attached to the tunnel walls; the rod was also supported just behind the plate by means of three wires. A sketch of the rig is given in Fig. 3.

For drag measurements, a small capacity-type balance was constructed and fitted between the rod and plate as shown in Fig. 3*.

Traverses behind the plates were made with pitot-static tubes and with a hot wire using the apparatus shown in Fig. 3. An elliptic-section tube spanned the tunnel and carried a sliding block which could be traversed and rigidly clamped in any position from outside the tunnel. Vertical movements were obtained by means of a length of streamlined rod clamped to the sliding block. The pitot-tubes and static-tubes were kept parallel to the tunnel axis. Measurements of the velocity near the axis of the plate were made with a pitot-static tube attached to the central rod, 0·6 in. from the axis of the plate. Reverse velocities were measured with this instrument pointing downstream.

The hot wire was kept normal to the tunnel axis. The associated electronic equipment which included a vibration analyser was basically that described in Refs. 4 and 5.

3. *Velocity Measurements.*—3.1. *Mean Velocities.*—Since the pitot-tubes and static-tubes were set parallel to, and the hot wire normal to the free stream, the velocity measurements are in error where the local stream is not parallel to the free stream. For the particular pitot-tubes and static-tubes used in these experiments, a check showed that the measured velocity exceeded the true velocity by 2 per cent for 10 deg misalignment and 6 per cent for 20 deg misalignment. Angular errors are small near the axis of the bubble and also near the position of its maximum width, so that the length and maximum diameter of the bubble are accurately determined.

---

* On the circular plate sufficient surface-pressure measurements were made (Fig. 10b) to obtain a drag coefficient by integration. The value obtained was 1·13, compared with 1·12 measured on the balance.

The hot wire measures the velocity component normal to its length. It was traversed in planes containing an axis of symmetry of the plate and the tunnel centre-line with the wire normal to the traverse plane. Velocity components in this plane are therefore obtained, and the component normal to such a plane should have an average value of zero.

Corrections for misalignments could not be applied as the mean flow directions were not determined.

The measurements are also subject to errors arising from the fluctuating nature of the flow behind the plates. Comparative traverses made with the pitot-tubes and static-tubes and with normal and inclined hot wires in a plane 18 in. behind the square plate are shown in Fig. 4 (the inclined hot wires were used in an attempt to establish the relative values of lateral and longitudinal velocity fluctuations, but the discrepancy shown in measuring mean velocity made the values of lateral fluctuation very doubtful and these are not given). These results were given in Ref. 1, where a small correction had been applied to the hot-wire measurements; in Fig. 4 of the present paper, the results are uncorrected. A correction to the hot-wire results for velocity fluctuation would bring the normal hot-wire values up to those of the pitot-static, but would scarcely change the disagreement between normal and inclined wires. Correction to the pitot-static results is not feasible, since over most of the traverses the velocity fluctuations are not known. Fig. 4 therefore merely shows the order of uncertainty of all the results presented in this paper, but this has no effect on the main conclusions.

3.2. *Velocity Fluctuations.*—The investigation of the longitudinal velocity fluctuations comprised measurements of the r.m.s. velocity fluctuation, u, and, at selected points, spectrum analyses of the fluctuations. The spectra are presented in the form of $n F(n)$ plotted against $\log n$, where n is the frequency (expressed non-dimensionally) and $F(n)$ is the spectrum function, defined so that $F(n) \, dn$ is the contribution to u^2/U_e^2 of frequencies between n and $n + dn$ (U_e is the free-stream speed corrected as discussed in Section 4).

The mean-square value of the velocity fluctuations $(u_{1,2})^2$, contained in a band of frequency between n_1 and n_2 is given by:

$$\frac{(u_{1,2})^2}{U_e^2} = \int_{n_1}^{n_2} F(n) \, dn$$

$$= \int_{n_1}^{n_2} n \, F(n) \, d(\log n)$$

and

$$\frac{u^2}{U_e^2} = \int_{n=0}^{n=\infty} n \, F(n) \, d(\log n).$$

The wave analyser used in the investigation had a band width Δn approximately equal to $0 \cdot 1 n$. Measurements were made of the mean square of the analyser output, Δu^2, over a range of frequency. Since the band width is small:

$$F(n) = \frac{\Delta u^2}{U_e^2} \Big/ \Delta n \text{ approximately}$$

and

$$n F(n) = \frac{\Delta u^2}{U_e^2} \Big/ \varepsilon_A,$$

where $\varepsilon_A = \Delta n/n$, the analyser band-width ratio.

4. *Blockage Corrections.*—The velocities behind the plates are given in terms of the uncorrected tunnel velocity, U_0, and are themselves uncorrected. The pressure co-efficients measured behind the plates are also uncorrected and are given in terms of the uncorrected tunnel dynamic head, $\frac{1}{2}\rho U_0^2$. This is because the wake blockage is known only at the plate.

3

Using the methods of Ref. 3, the drag coefficients and base-pressure coefficients have been corrected for blockage, and the limiting values of the pressure coefficient at an infinite distance behind the plates have been estimated and are indicated in Fig. 11b. The blockage correction varies from 2·4 per cent on velocity for the square plate to 1·7 per cent for the 20 : 1 aspect-ratio plate.

In making velocity fluctuations and frequencies non-dimensional, the true wind speed is used. Since, with the frequency analyser used, the accuracy of frequency measurement is about ± 2 per cent, it was not considered necessary in deducing the true wind speed to make allowances for:

(a) the day to day variations in barometric pressure and temperature (less than ± 1 per cent on velocity)

(b) the variations in uncorrected tunnel dynamic head (less than ± 0·5 per cent on velocity)

(c) the differences in blockage corrections between plates (less than ± 0·4 per cent on velocity).

Accordingly, a mean blockage correction on velocity of 2 per cent has been taken, with an additional 1½ per cent correction for the prevailing low pressures associated with the type of tunnel used. These corrections applied to the average uncorrected tunnel speed of 140 ft/sec give an effective tunnel speed (U_e) of 145 ft/sec and this has been used throughout in forming the non-dimensional frequencies and fluctuating velocities. ,

5. *Results.*—5.1. *Presentation.*—The results are presented in non-dimensional form. The areas used are the total solid areas of the plates.

The best choice of a representative length varies as follows:

(1) For the low-aspect-ratio plates, the square root of the area, $\sqrt{S}$, is the most useful parameter, and has been used.

(2) For the two-dimensional plate, and for making comparisons between high-aspect-ratio plates and the two-dimensional plate, the chord, c, is used.

(3) In Fig. 11 the characteristics of bubbles are compared on the basis of bubble length, X.

(4) In Fig. 10 the spanwise distributions of base pressure on various plates are compared in terms of the semi-span, $b/2$.

(5) In order to form a consistent series of Strouhal Numbers in Table 2, both dimensions of the plate have been used as indicated in the Table.

5.2. *Effects of Aspect Ratio (Rectangular Plates).*—The effects of aspect ratio are summarised in Tables 1 and 2 and Figs. 9a to 9d; the drag coefficient and base-pressure coefficient quoted for a two-dimensional plate are due to Fage and Johansen[6] corrected for blockage by the methods of Ref. 3. As the aspect ratio is increased (from unity), the drag coefficient rises, the base pressure falls and the bubble length decreases. These changes are relatively small up to an aspect ratio of 10; thereafter the changes with aspect ratio are more rapid.

The base pressure (— 0·36) is uniformly distributed at $A = 1$; as the aspect ratio is increased, the drop in base pressure occurs first towards the tips (Fig. 10). At $A = 20$ the base pressure is fairly uniform at — 0·6 over the middle half of the span, with a sharp drop near the tips. The level of the pressure over the middle half of the span, although lower than on the lower aspect-ratio plates, is considerably higher than on the two-dimensional plate. Correspondingly the bubble length (expressed in terms of the chord) is 4·29 for $A = 20$ and 2·82 for $A = \infty$.

Behind the low-aspect-ratio plates (Figs. 5a to 5d) it will be seen that, at any one distance behind the plate, the static pressure is fairly constant within the bubble. There are static-pressure gradients between the bubble boundary and the total-head boundary and also down the length of the bubble.

4

Axial distributions of total head, static pressure and velocity are shown in Figs. 11a to 11c for all the rectangular plates. Between $A = 1$ and $A = 10$ the bubble length decreases from $2 \cdot 96\sqrt{S}$ to $2 \cdot 26\sqrt{S}$ but the distributions of pressure and velocity within the bubble do not change much. The static-pressure coefficient in the centre of the downstream face of the plate is $- 0 \cdot 42^*$. At the mid-length of the bubble the static-pressure coefficient has fallen to about $- 0 \cdot 62$; pressure recovery then commences and is complete just behind the end of the bubble. The maximum reverse velocity in the bubble is from $0 \cdot 43 U_0$ to $0 \cdot 55 U_0$, depending on the aspect ratio.

At aspect ratios of 20 and ∞ the general levels of static pressure within the bubbles are lower, and pressure recovery is far from complete at the ends of the bubbles.

The plate of aspect ratio 10 is of interest in that it is of about the highest aspect ratio which retains markedly three-dimensional characteristics. A series of pitot-static traverses were therefore made at several distances behind this plate in order to illustrate the development of the total-head boundary. The results are shown in Fig. 7, where it will be seen that the cross-section of the wake changes from an oval immediately behind the plate to a substantially circular shape at $x/\sqrt{S} = 3 \cdot 60$ (about $1\frac{1}{2}$ bubble lengths). In contrast, the shape of the wake behind the plate of aspect ratio 20 (Fig. 8), also at $x/\sqrt{S} = 3 \cdot 60$, is substantially rectangular.

The unsteadiness of these flow patterns was investigated by measuring the longitudinal velocity fluctuations with a hot wire set normal to the tunnel axis. Spanwise and chordwise traverses were made at a distance behind each plate equal to about $1\frac{1}{4}$ bubble lengths. The results are shown in Fig. 12. Near the axis of each plate there are velocity fluctuations of large amplitude which increase with distance from the axis to a maximum (u/U_e of the order of $0 \cdot 2$), at a point well inside the wake and then fall rapidly with further movement outwards. Up to $A = 10$ the chordwise and spanwise distributions do not differ much; at $A = 20$ the high velocity fluctuations have spread significantly in the spanwise direction and contracted in the chordwise direction.

Fig. 12 also shows spectra of the velocity fluctuations measured at the points where u/U_e is a maximum. Most of the spectra show high peak values of $n F(n)$† at particular values of n. Such a peak indicates the presence of a regular shedding of turbulent eddies from the plate. The values of these shedding frequencies are collected in Table 2. Outside the wake, although the velocity fluctuations are very small, a shedding frequency is usually more clearly defined than inside the wake. The shedding frequencies quoted in Table 2 are therefore taken from spectra measured outside the wake (at points indicated in the Table).

Up to an aspect ratio of 10, two shedding frequencies can be distinguished outside the wake for each plate (except the square plate), one associated with the smaller dimension of the plate and a lower frequency associated with the larger dimension. At aspect ratio 5 only, the spectrum measured near the tip of the plate showed both frequencies. In all other cases, the spectra measured near the tips showed only the lower shedding frequencies and the spectra measured near the centre of the span showed only the higher frequencies. The results, expressed in non-dimensional form, are plotted in Fig. 9 where for plates of aspect ratio less than 1 the larger dimension of the plate is used as the chord. Between $A = 0 \cdot 5$ and $A = \infty$ the Strouhal Number (fc/U_e) varies between $0 \cdot 086$ and $0 \cdot 145$. Between $A = 0 \cdot 5$ and $A = 0 \cdot 1$ the Strouhal Number increases considerably but the shedding frequencies for $A = 0 \cdot 2$ and $0 \cdot 1$ were not well defined.

5.3. *Effects of Shape of Plate.*—It became clear from the early measurements of Ref. 1 on square, circular and equilateral-triangular plates that the flow pattern was little affected by the shape. Contours of constant velocity behind these plates, taken from Ref. 1, are shown in Fig. 6

---

* Uncorrected for blockage.

† The shapes (including the heights) of the peaks are determined by the characteristics of the analyser. Strictly, the results should be presented in the form of the continuous spectrum (an example is shown in Fig. 12b) and the mean-square value of the velocity fluctuation at the single frequency. For the present purpose it is sufficient to recognise the existence of peaks.

5

of the present note. An attempt to alter the bubble was therefore made by fitting tabs around the circumference of a circular plate (Fig. 2). The results obtained on all of these plates are summarised in the following Table:

Shape of plate	Area S (sq in.)	C_D	C_{Pb}	$\dfrac{X}{\sqrt{S}}$	$\dfrac{f\sqrt{S}}{U_e}$
Square	25·0	1·14	—0·36	2·95	0·115
Circular ..	25·1	1·12	—0·36	2·92	0·115
Triangular ..	25·0	1·15	—	2·82	0·115
Tabbed	18·6	1·12	—0·36	3·04	0·117

and more detailed comparisons of the nature of the flows are given in Figs. 13 to 15. These results differ by little more than the experimental accuracy. It is concluded that large charges in the shape of the plate have only negligible effects on the aerodynamic characteristics.

Ref. 2 shows, however, that perforating the plate can prevent the formation of a bubble, and hence suppress the regular shedding of eddies and much of the random low-frequency velocity fluctuation.

6. *Conclusions.*—The effects of aspect ratio on drag, base pressure and flow pattern are small up to $A = 10$. All the plates shed turbulent eddies at particular frequencies; generally there are two shedding frequencies for each rectangular plate, one associated with the smaller dimension of the plate and a lower frequency associated with the longer dimension.

Large charges in the shape of low-aspect-ratio plates have very small effects on the aerodynamic characteristics but the regular shedding of eddies can be eliminated by perforating the plate; this is accompanied by a reduction in the random low-frequency velocity fluctuations.

LIST OF SYMBOLS

c — Chord of plate

b — Span of plate

S — Area of plate (*see* Section 5.1)

l — Representative length (*see* Section 5.1)

A — Aspect ratio of plate

x — Longitudinal distance (measured from front surface of plate)

y — Lateral distance (measured from centre-line of plate)

z — Vertical distance (measured from centre-line of plate)

r — Radial distance measured from centre-line of plate

R — Radius of circular plate

X — Length of bubble

H — Total head

P — Static pressure

C_{Pb} — Base-pressure coefficient

U_0 — Tunnel speed (uncorrected for blockage)

U_e — Effective tunnel speed (*see* Section 4)

U — Mean local velocity

u^2 — Mean-square value of longitudinal velocity fluctuation

f — Frequency (c/sec)

$n = \dfrac{fl}{U_e}$

Strouhal Number = Value of n corresponding to regular shedding of eddies, *i.e.*, to a peak in a spectrum

Δn — Analyser band width

$\varepsilon_A = \dfrac{\Delta n}{n}$ = Analyser band-width ratio

Δu^2 — Mean-square value of velocity fluctuations passed by analyser

$n\,F(n) = \dfrac{\Delta u^2}{U_e^2}\Big/ \varepsilon_A$ (*see* Section 3)

$\psi = \dfrac{1}{U_0 S}\int U 2\pi r\, dr$ = Stream function

7

REFERENCES

No.	Author	Title, etc.
1	R. Fail, T. B. Owen and R. C. W. Eyre	Preliminary low-speed wind-tunnel tests on flat plates and air brakes: Flow, vibration and balance measurements. C.P. 251. January, 1955.
2	B. G. de Bray	Low-speed wind-tunnel tests on perforated square flat plates normal to the air stream. Drag and velocity fluctuation measurements. C.P. 323. October, 1956.
3	E. C. Maskell	A theory of wind-tunnel blockage effects on stalled flows. R.A.E. Report (To be issued.)
4	R. H. James and J. H. Mitchell ..	Turbulence measuring apparatus. R.A.E. Tech. Note Inst. 949. A.R.C. 9885. March, 1946.
5	H. Schuh and K. G. Winter	R.A.E. 4 ft × 3 ft Experimental Low Turbulence Wind Tunnel. Part II.—Measurements of longitudinal intensity of turbulence. R.A.E. Report Aero. 2285. A.R.C. 11,829. August, 1948.
6	A. Fage and F. C. Johansen	On the flow of air behind an inclined flat plate of infinite span. R. & M. 1104. 1927.

TABLE 1

Drag, Base Pressure and Bubble Length of Rectangular Flat Plates
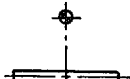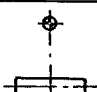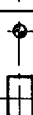
A	Chord c (in.)	Span b (in.)	Bubble length X (in.)	$\dfrac{X}{\sqrt{S}}$	$\dfrac{X}{c}$	C_D	C_{Pb}*
1	5·00	5·00	14·8	2·96	2·96	1·143	—0·360
2	3·54	7·07	14·3	2·86	4·04	1·15	—0·37
5	2·24	11·2	12·3	2·46	5·49	1·22	—0·415
10	1·58	15·8	11·3	2·26	7·15	1·27	—0·47
20	1·12	22·35	4·8	0·96	4·29	1·50	—0·68
∞†	1·24	∞	3·5	—	2·82	1·86	—1·08

* Mean values given for plates on which the base pressure varies across the span (Fig. 10).

† The drag and base pressure are taken from Ref. 6 and corrected for blockage by the method of Ref. 3.

TABLE 2

Shedding Frequencies of Rectangular Flat Plates Measured at $x = 3\cdot6\sqrt{S}$ *behind Plates Placed with Longer Side Horizontal in 4 ft × 3 ft Tunnel*

A	Frequencies measured at points indicated thus ⊕	Chord c (in.)	Span b (in.)	$\dfrac{fc}{U_e}$	$\dfrac{f\sqrt{S}}{U_e}$	Remarks
∞		1·24	∞	0·145*	—	Sharply defined shedding frequencies
20		1·12	22·35	0·109	0·487	
10		1·58	15·80	0·086	0·272	
5		2·24	11·20	0·093	0·208	
2		3·54	7·07	0·100	0·141	
1		5·00	5·00	0·115	0·115	
$\dfrac{1}{2}$		7·07	3·54	0·141	0·100	
$\dfrac{1}{5}$		11·20	2·24	0·205 0·457	0·092 0·204	Poorly defined shedding frequencies
$\dfrac{1}{10}$		15·80	1·58	0·612	0·193	
$\dfrac{1}{20}$		22·35	1·12	—	—	No evidence of regular shedding

* Shedding frequency for two dimensional plate measured at x = 3·63c behind plate placed vertically in tunnel.

11
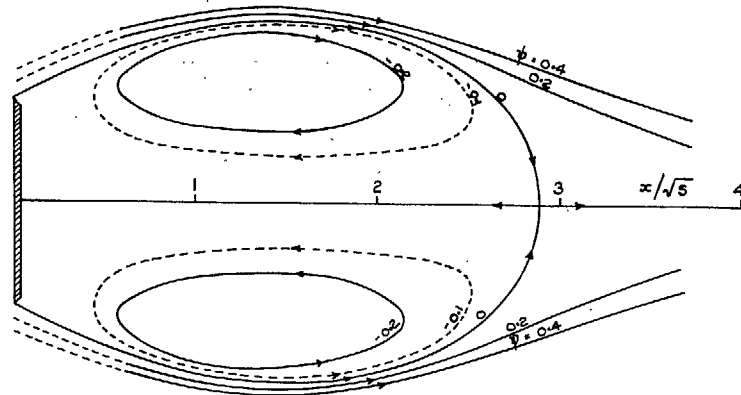
(a) STREAMLINES BEHIND PLATE.

WAKE BOUNDARY

BUBBLE BOUNDARY
($\psi=0$, FIG.I (a))

$x/\sqrt{s}$
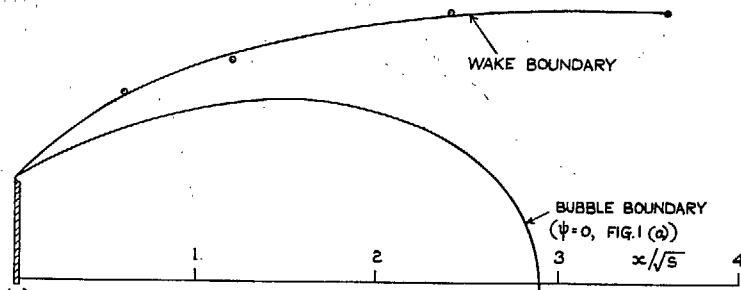
(b) COMPARISON OF BUBBLE AND TOTAL HEAD BOUNDARIES.

ALONG WAKE BOUNDARY.

THIS POINT IS CORRECTED
FOR MISALIGNMENT OF
PRESSURE TUBE (SEE section 3·1)

$\dfrac{P}{\frac{1}{2}\rho U_o^2}$

NEAR AXIS OF PLATE.
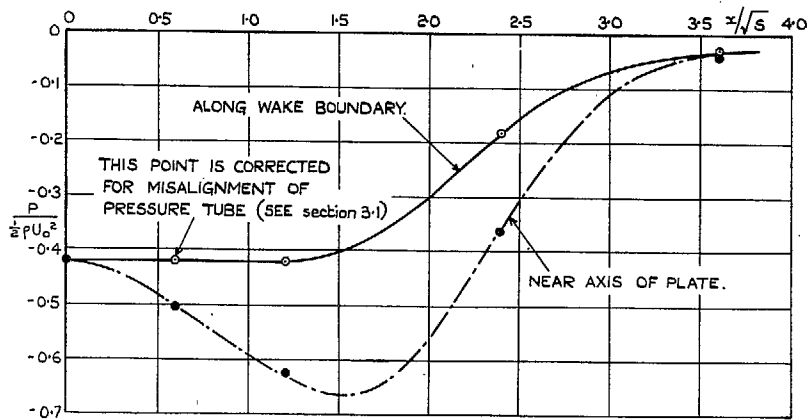
(c) STATIC PRESSURE DISTRIBUTION.

FIGS. 1a to 1c.   Mean flow behind circular plate.
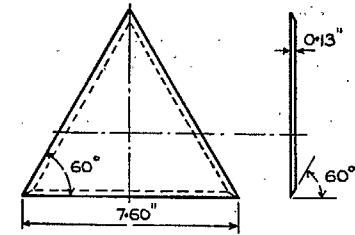
TRIANGULAR PLATE
S = 25 SQ. IN.
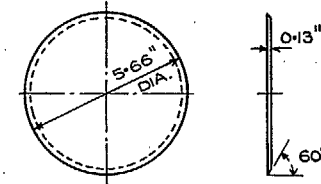
CIRCULAR PLATE
S = 25·1 SQ. IN.
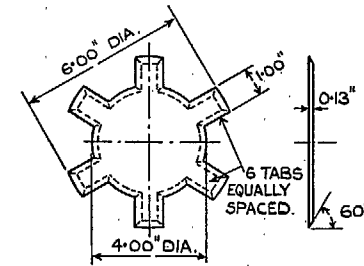
TABBED PLATE
S = 18·6 SQ. IN.
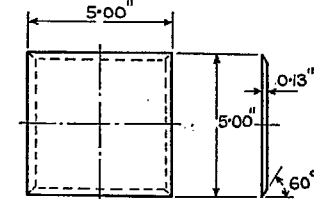
SQUARE PLATE
S = 25 SQ. IN.

FIG. 2.   Details of flat
plates.

HOLDER FOR PITOT- STATIC
OR HOT- WIRE.

BRACING
WIRES.

WIND

SLIDING
BLOCK.

TRAVERSING ROD.

MAIN SUPPORT TUBES
(STREAMLINE SECTION)

CLAMPING ROD.
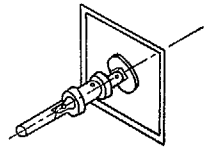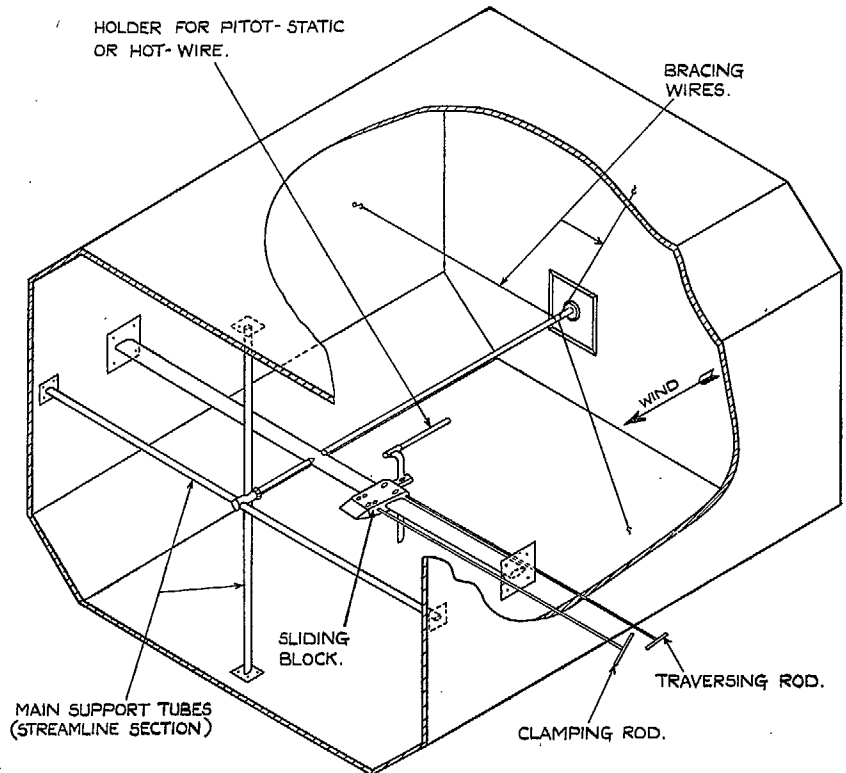
SQUARE PLATE MOUNTED
ON DRAG BALANCE.

FIG. 3.   Arrangement of apparatus.   Tests on flat plates in 4 ft × 3 ft
Wind Tunnel.

$\frac{u}{U_o}$

PITOT- STATIC MEASUREMENTS. ⊙

NORMAL HOT WIRE ▫

INCLINED HOT WIRE x

DISTANCE FROM ℄ OF PLATE (IN)
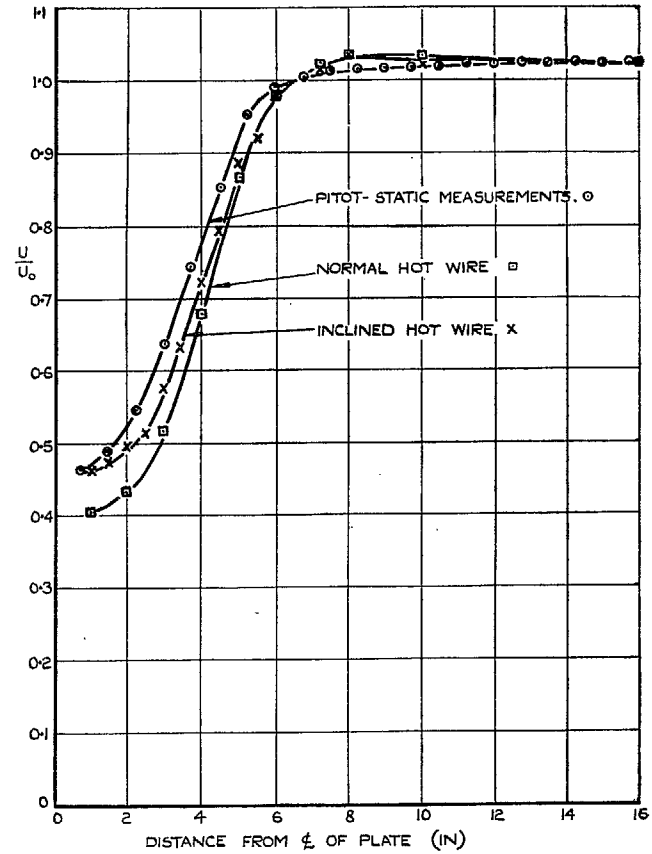
(a) COMPARISON OF HOT WIRE AND PITOT-STATIC
MEASUREMENT OF VELOCITY.

ANGLE OF YAW
(INWARDS)

DISTANCE FROM ℄ OF PLATE (IN)
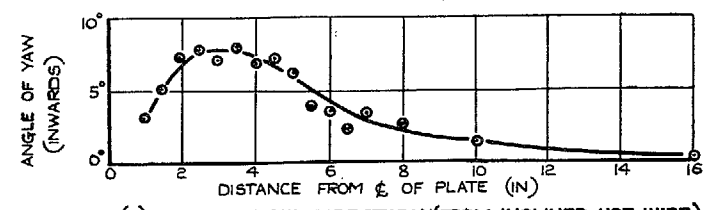
(b) LOCAL FLOW DIRECTION (FROM INCLINED HOT WIRE.)

FIGS. 4a and 4b.   Comparative hot-wire and pitot-
static traverses behind square plate $(x/\sqrt{S} = 3\cdot60,$
$S = 25$ sq in.).
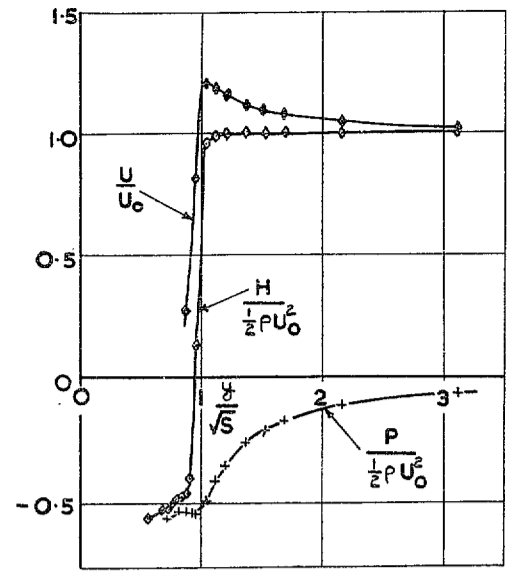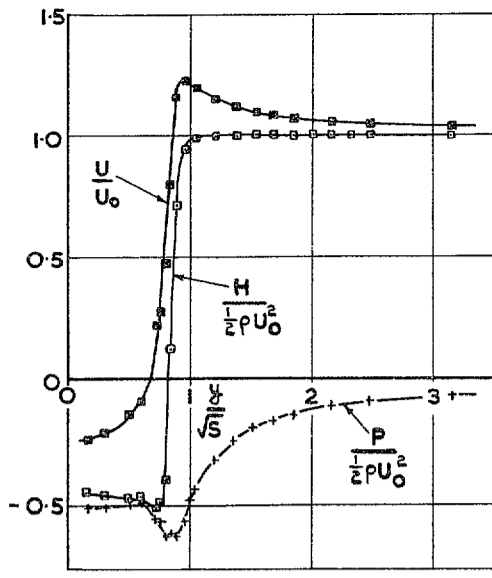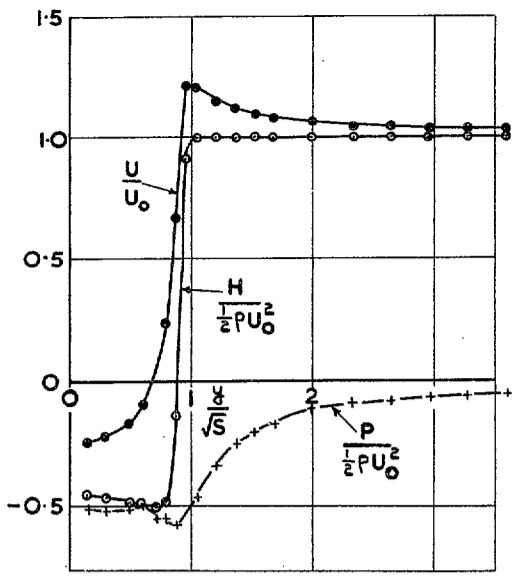
$$\frac{x}{\sqrt{S}} = 0.6, \quad \frac{x}{X} = 0.203.$$
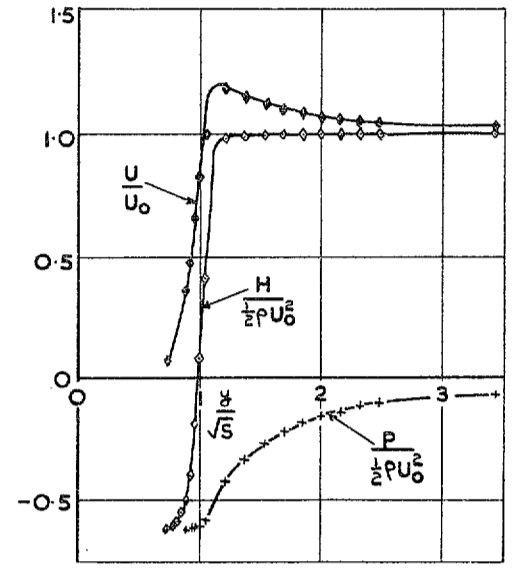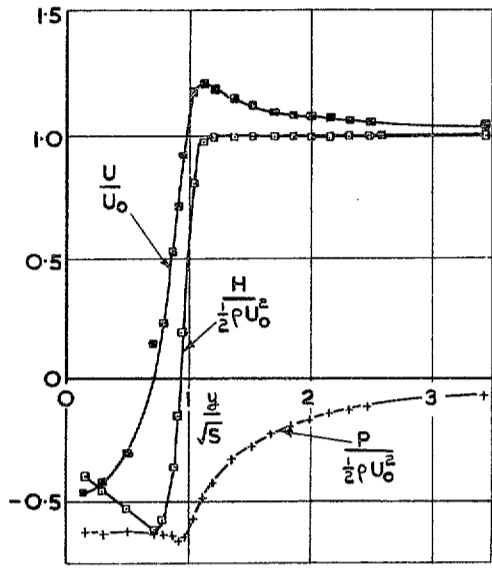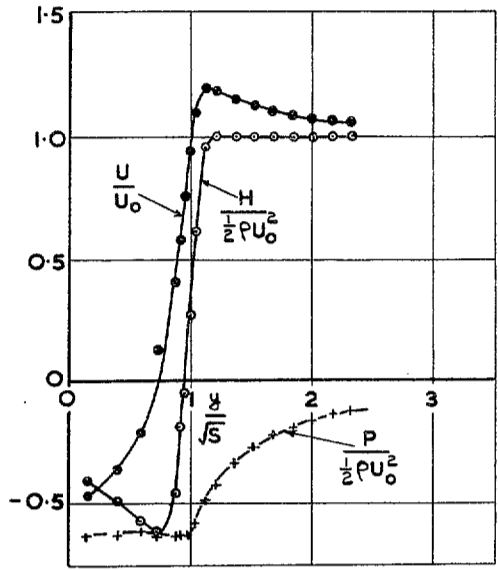
$$\frac{x}{\sqrt{S}} = 1.2, \quad \frac{x}{X} = 0.406.$$
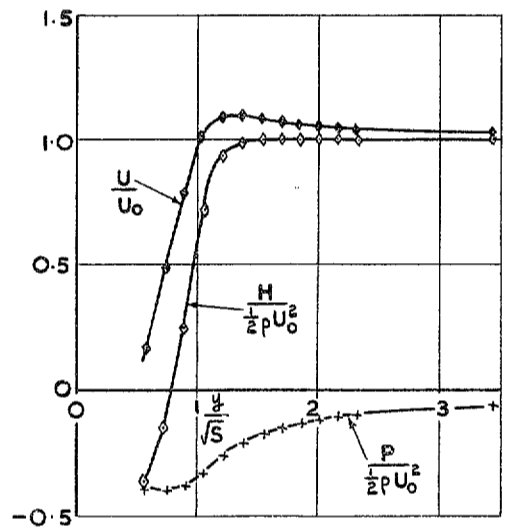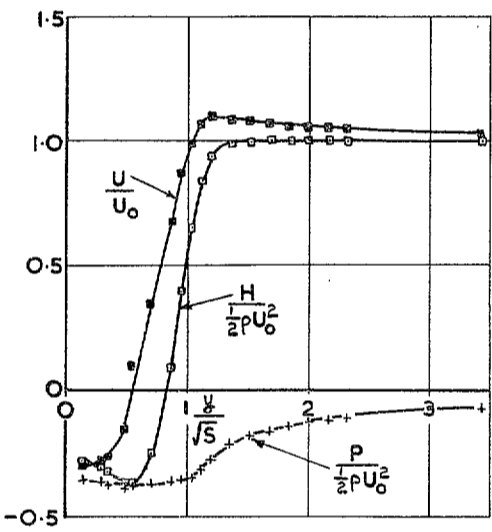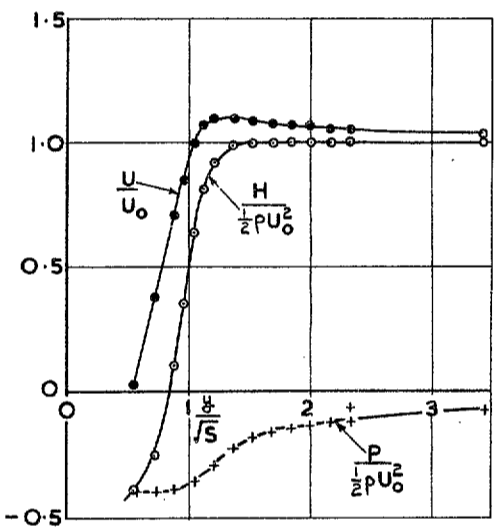
$$\frac{x}{\sqrt{S}} = 2.4, \quad \frac{x}{X} = 0.812.$$
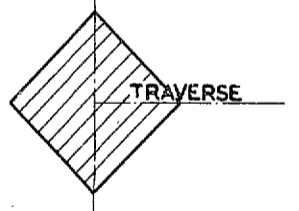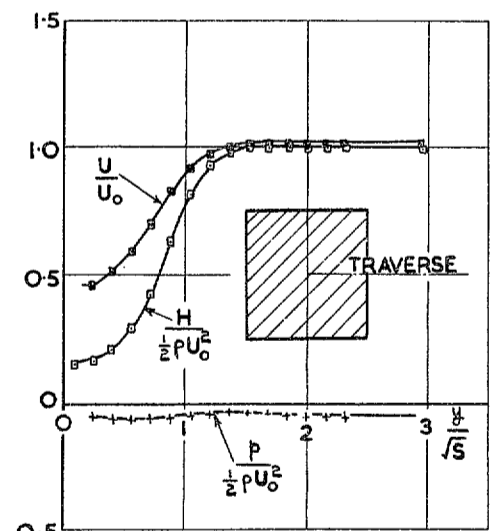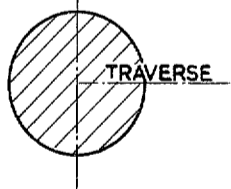
$$\frac{x}{\sqrt{S}} = 3.6, \quad \frac{x}{X} = 1.218.$$
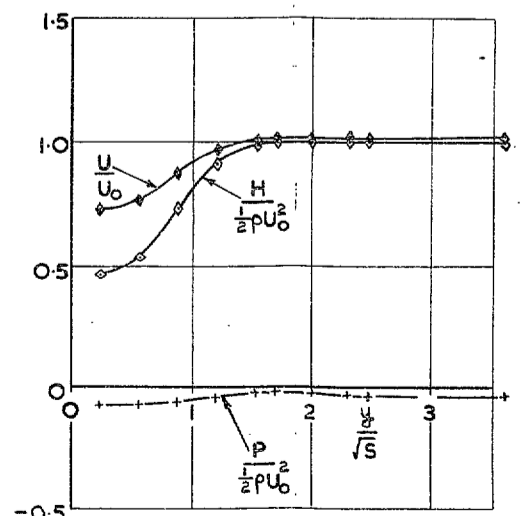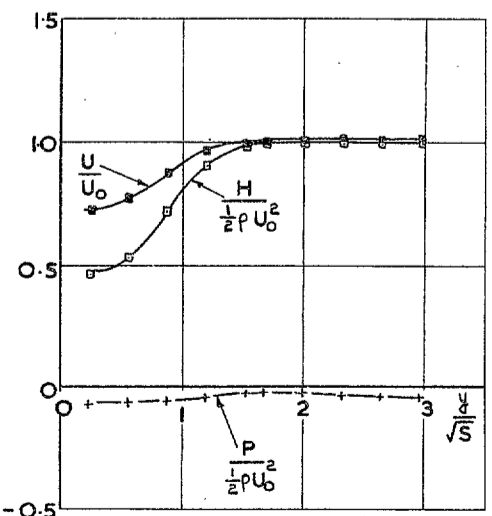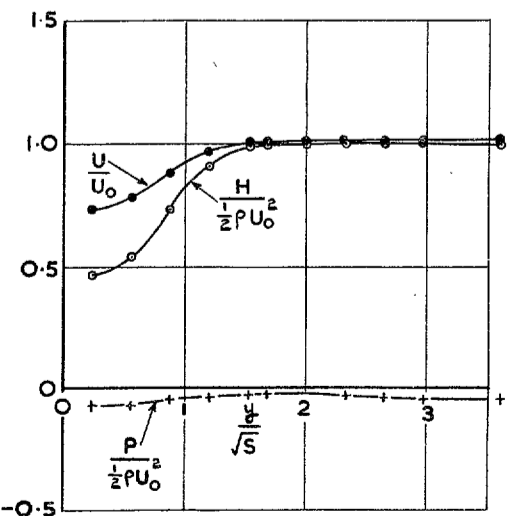
$$\frac{x}{\sqrt{S}} = 4.8, \quad \frac{x}{X} = 1.624.$$

(a) CIRCULAR PLATE.   (b) SQUARE PLATE.

FIGS. 5a and 5b.   Flow behind flat plates ($S = 25$ sq. in.). — Total head, static pressure and velocity distribution.
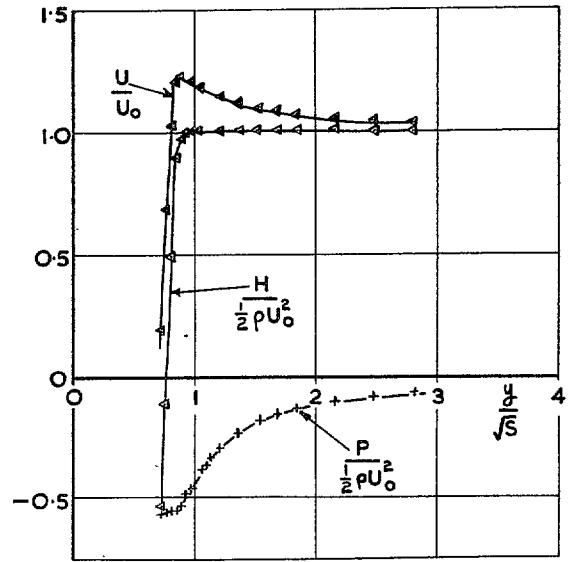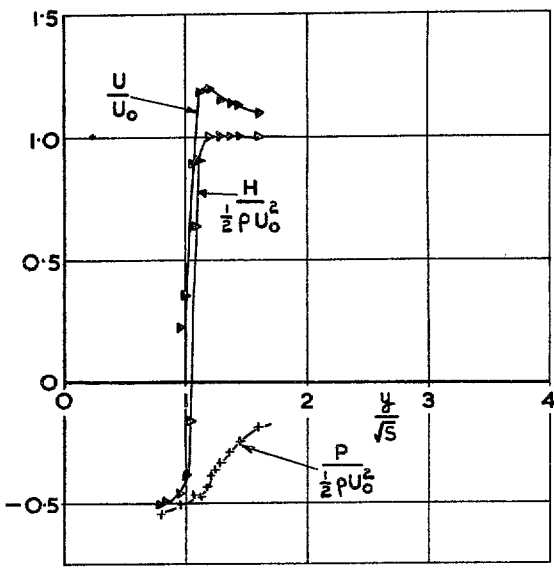
$$\frac{x}{\sqrt{S}} = 0.6, \quad \frac{x}{X} = 0.213.$$
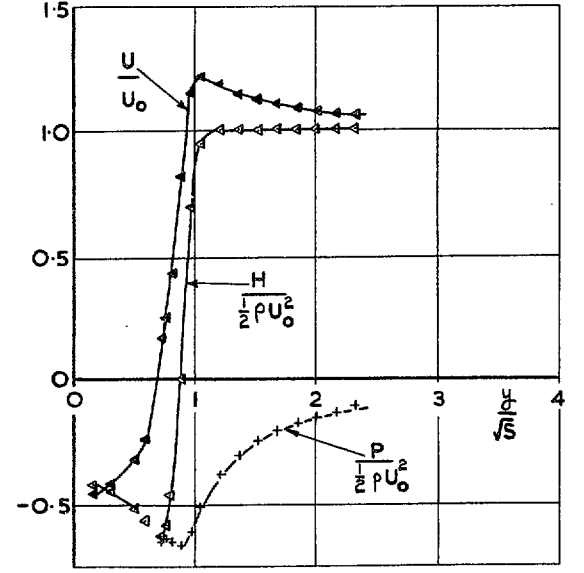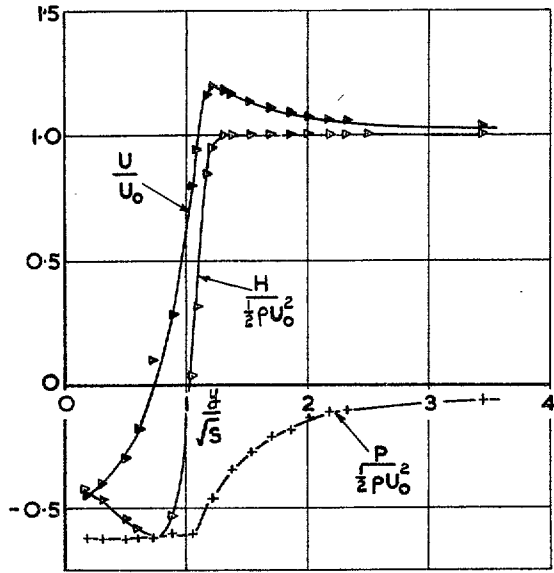
$$\frac{x}{\sqrt{S}} = 1.2, \quad \frac{x}{X} = 0.426.$$

$$\frac{x}{\sqrt{S}} = 2.4, \quad \frac{x}{X} = 0.85.$$

TRAVERSE
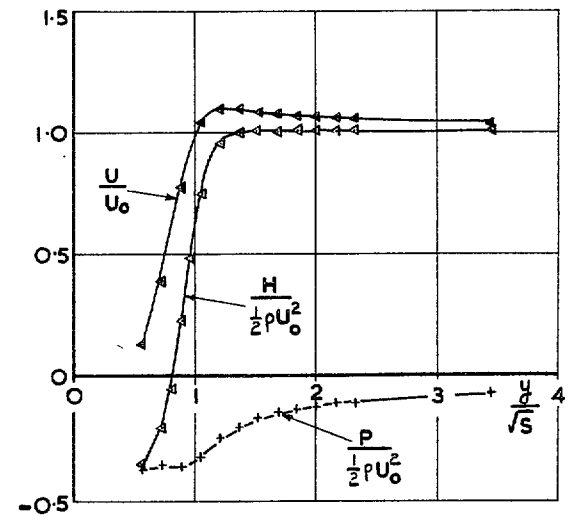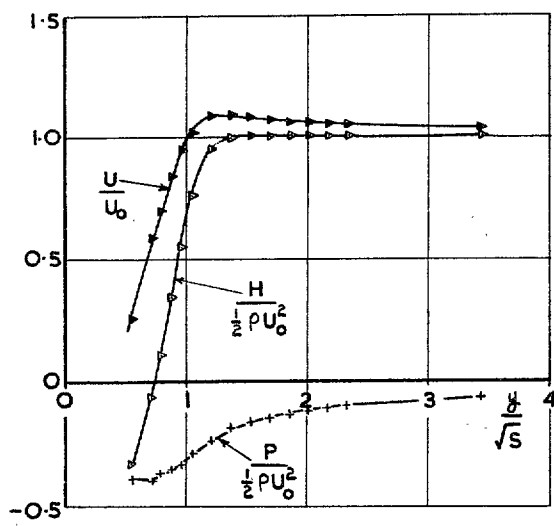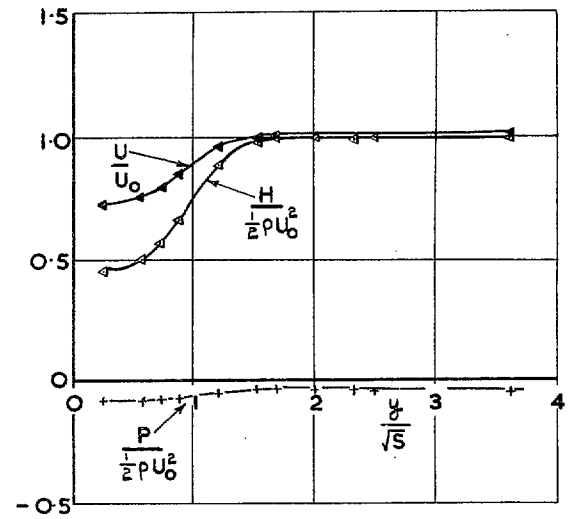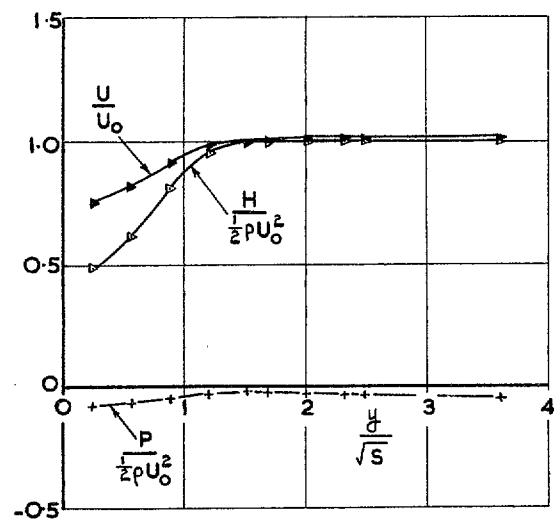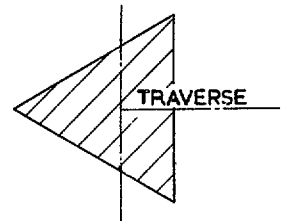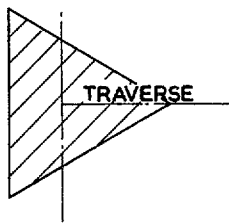
$$\frac{x}{\sqrt{X}} = 4.8, \quad \frac{x}{X} = 1.70.$$

(c) TRIANGULAR PLATE.

FIG. 5c.   Flow behind flat plate ($S = 25$ sq. in.). — Total head, static pressure and velocity distribution.
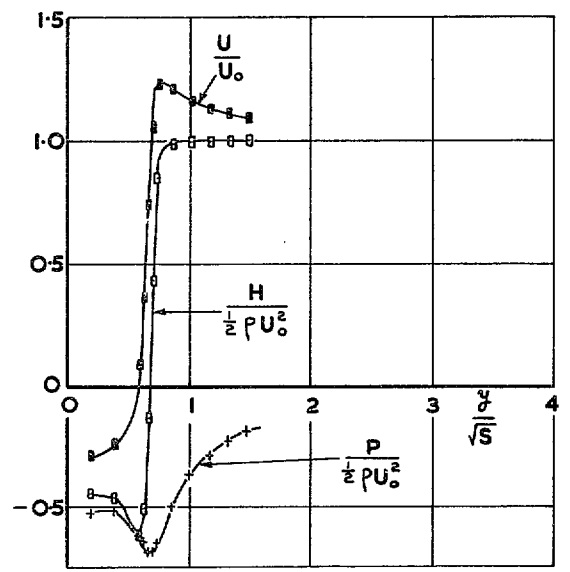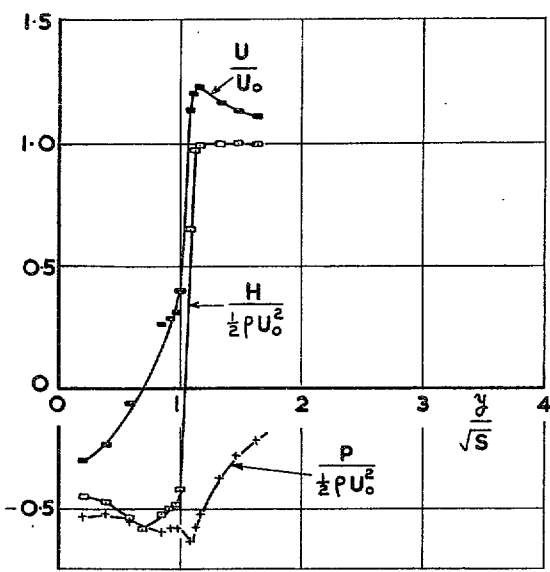
$$\frac{x}{\sqrt{S}} = 0.577, \quad \frac{x}{X} = 0.203.$$
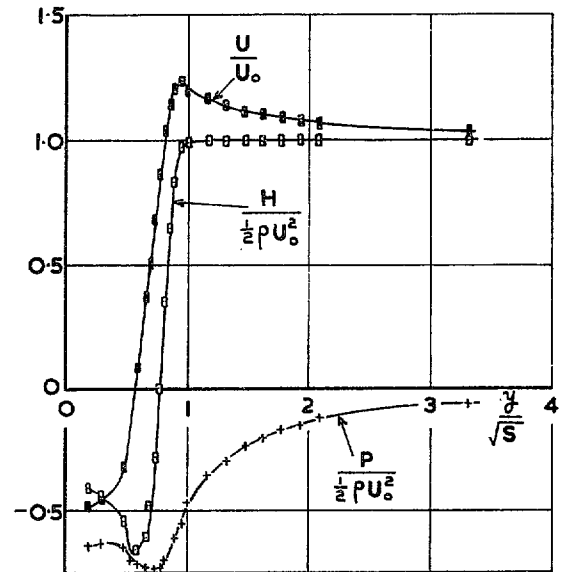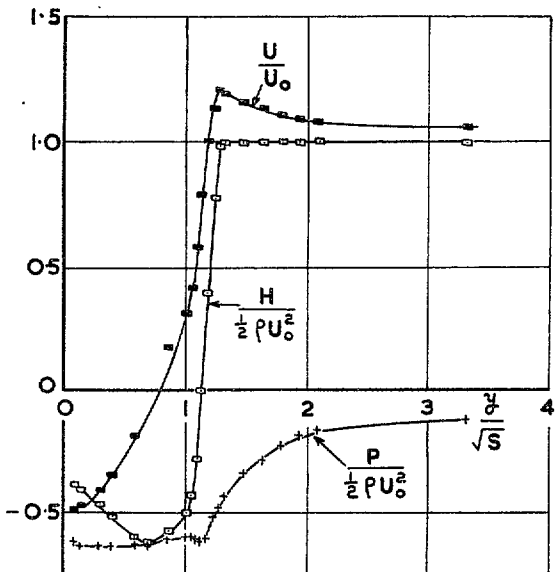
$$\frac{x}{\sqrt{S}} = 1.154, \quad \frac{x}{X} = 0.406.$$
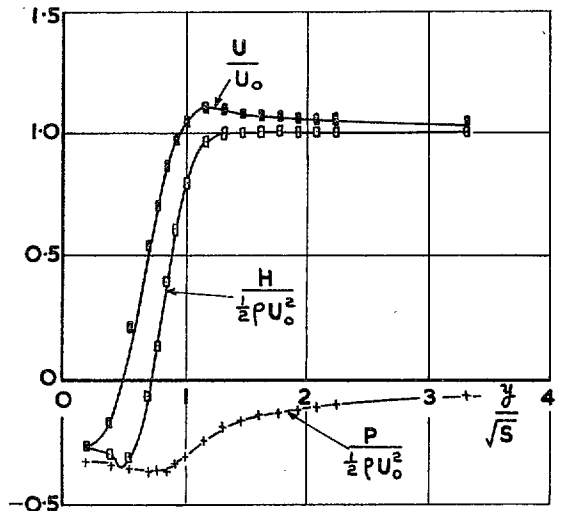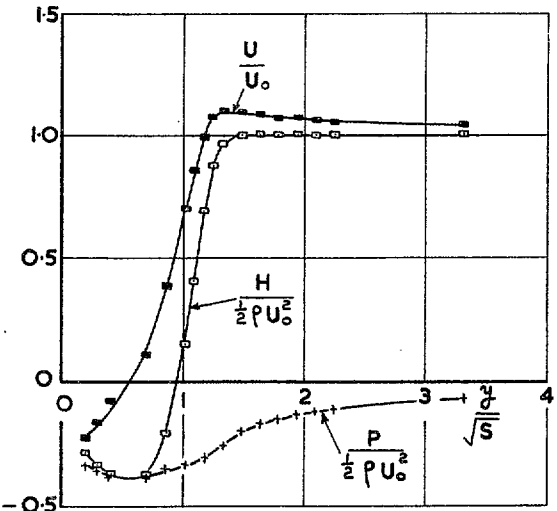
$$\frac{x}{\sqrt{S}} = 2.310, \quad \frac{x}{X} = 0.812.$$
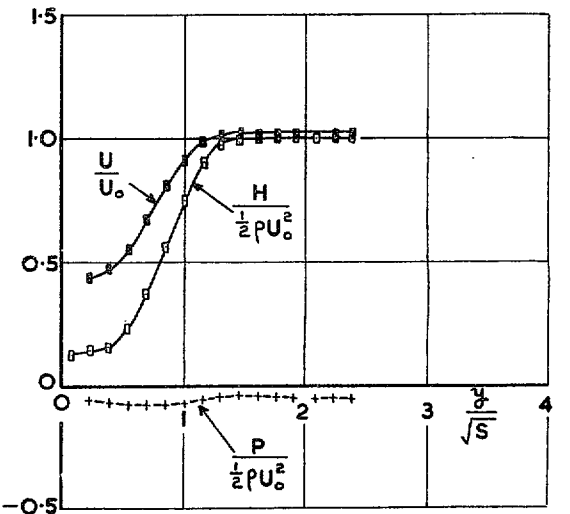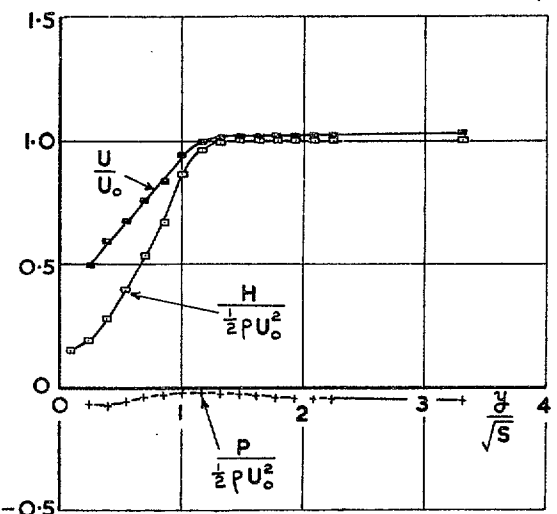
$$\frac{x}{\sqrt{S}} = 3.464, \quad \frac{x}{X} = 1.218.$$
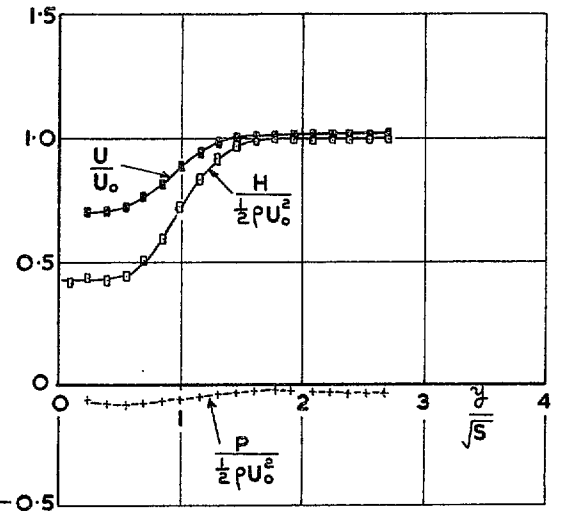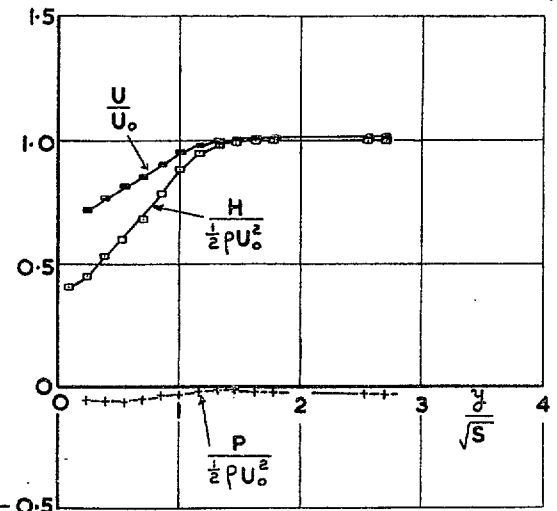
$$\frac{x}{\sqrt{S}} = 4.618, \quad \frac{x}{X} = 1.624.$$
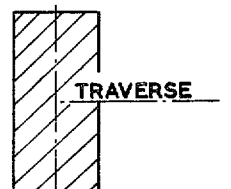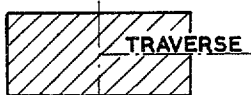
(d) RECTANGULAR PLATE A = 2·15.

FIG. 5d. Flow behind flat plate ($S = 27$ sq. in.). — Total head, static pressure and velocity distribution.
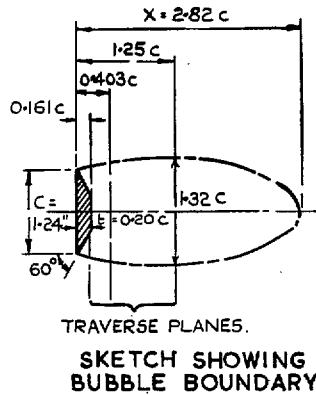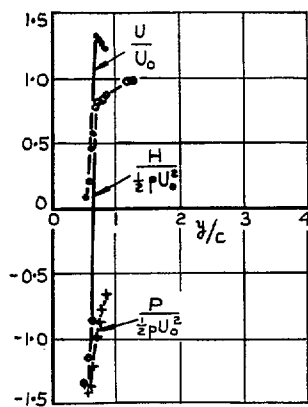
$\frac{x}{c} = 0.161, \quad \frac{x}{X} = 0.057.$
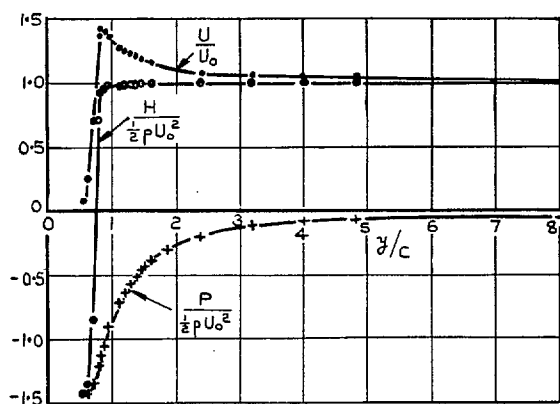
$\frac{x}{c} = 0.403, \quad \frac{x}{X} = 0.143$
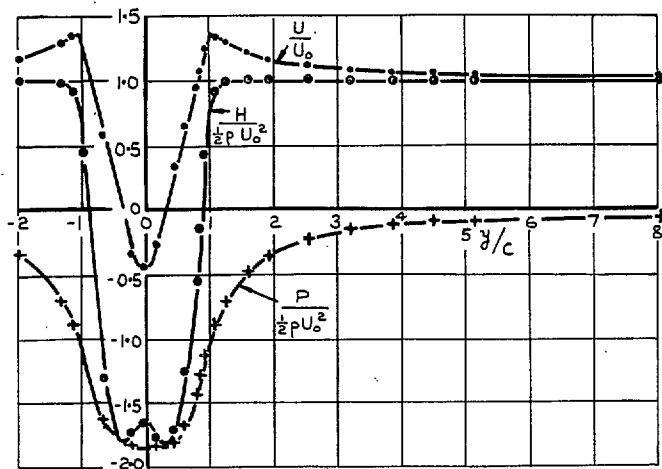
$\frac{x}{c} = 1.25, \quad \frac{x}{X} = 0.442.$

(e) TWO DIMENSIONAL PLATE (C = 1.24 IN.)

FIG. 5e.   Flow behind flat plates.—Total head, static
pressure and velocity distribution.

13
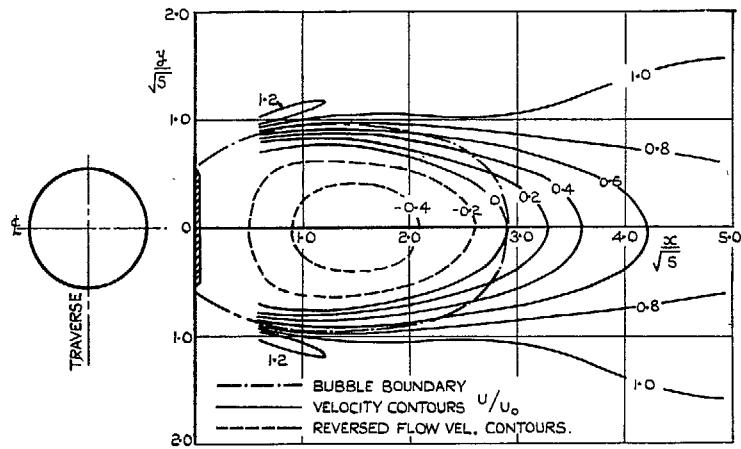
(a) CIRCULAR PLATE (S = 25·1 SQ. IN.)
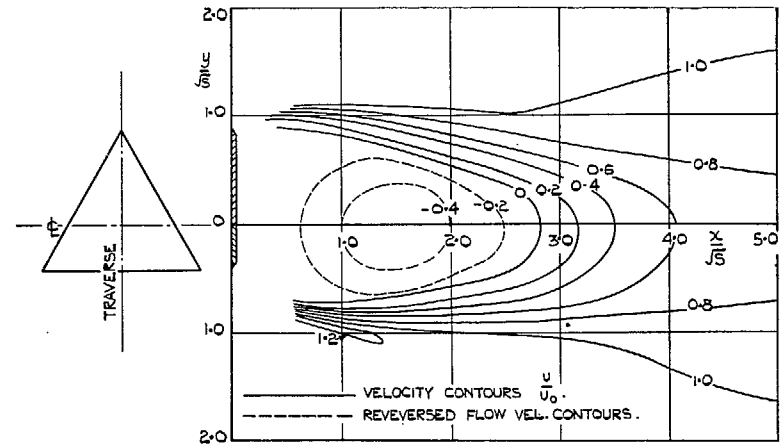
(C) TRIANGULAR PLATE (S = 25·0 SQ. IN.)
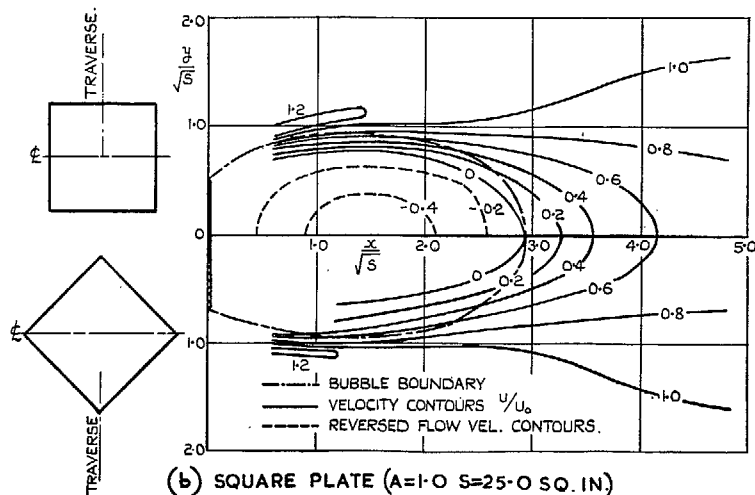
(b) SQUARE PLATE (A = 1·0 S = 25·0 SQ. IN.)
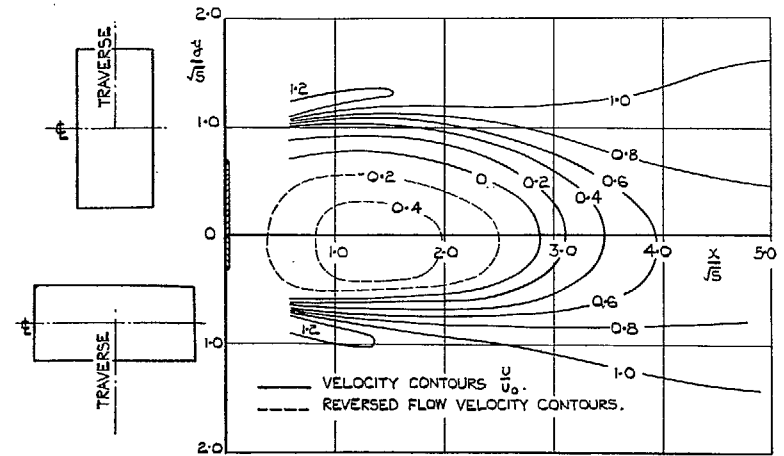
(d) RECTANGULAR PLATE (A = 2·15, S = 27·0 SQ. IN.)

FIGS. 6a to 6d.   Flow behind flat plates.—Velocity contours.
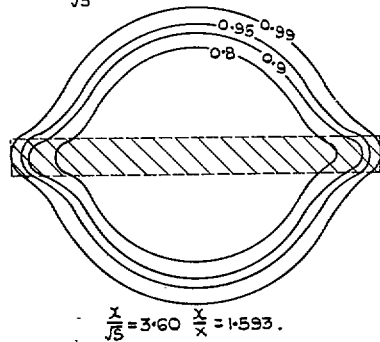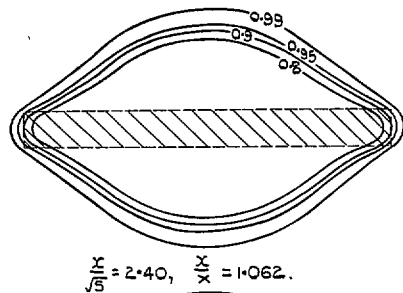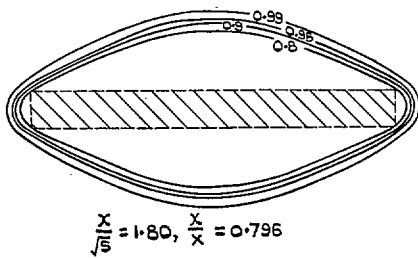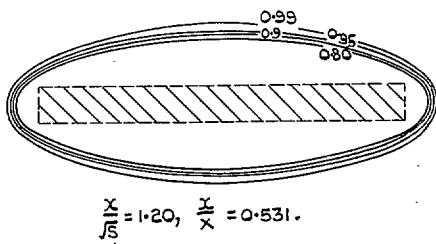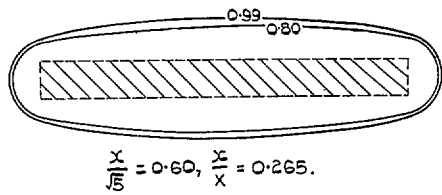
FIG. 7a.   Flow behind flat plate of aspect ratio 10.—Contours of $H/\frac{1}{2}\rho U_0^2$ behind plate.
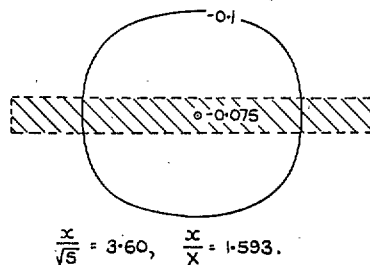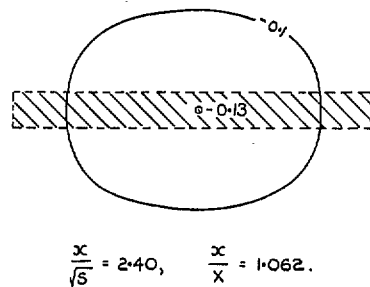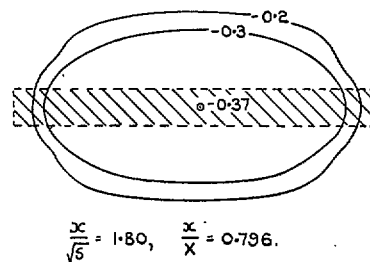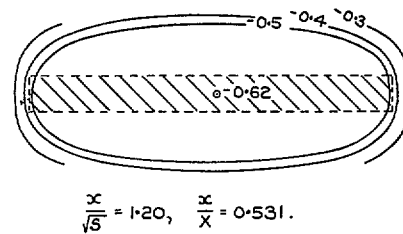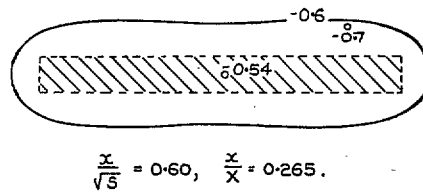
FIG. 7b.   Flow behind flat plate of aspect ratio 10.—Contours of $P/\frac{1}{2}\rho U_0^2$ behind plate.

15

$\frac{x}{\sqrt{S}} = 0.60, \quad \frac{x}{X} = 0.265.$

$\frac{x}{\sqrt{S}} = 1.20, \quad \frac{x}{X} = 0.531.$

$\frac{x}{\sqrt{S}} = 1.80, \quad \frac{x}{X} = 0.796.$

$\frac{x}{\sqrt{S}} = 2.40, \quad \frac{x}{X} = 1.062.$

$\frac{x}{\sqrt{S}} = 3.60, \quad \frac{x}{X} = 1.593.$
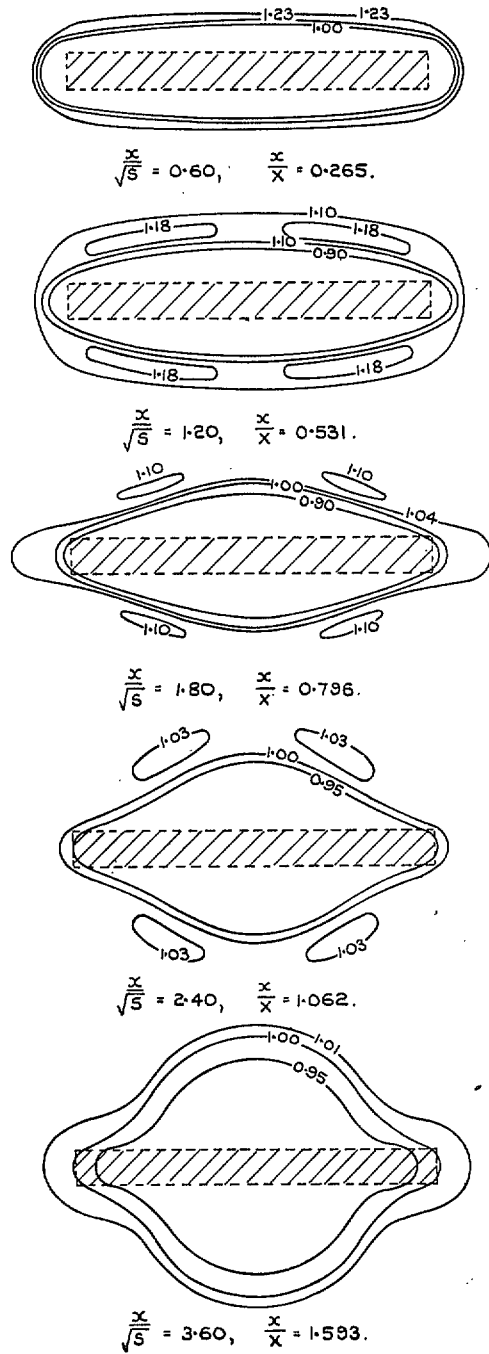
FIG. 7c. Flow behind flat plate of aspect ratio 10.—Contours of U/U_0 behind plate.
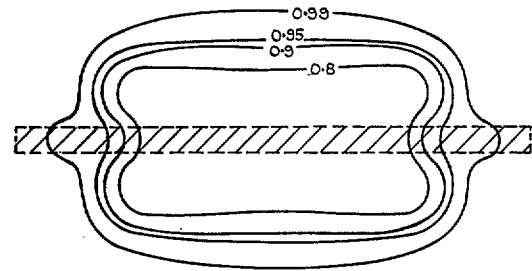
(a) TOTAL HEAD $\frac{H}{\frac{1}{2}\rho U_o^2}$
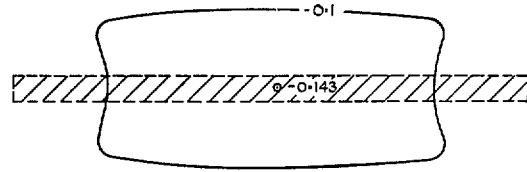
(b) STATIC PRESSURE $\frac{P}{\frac{1}{2}\rho U_o^2}$
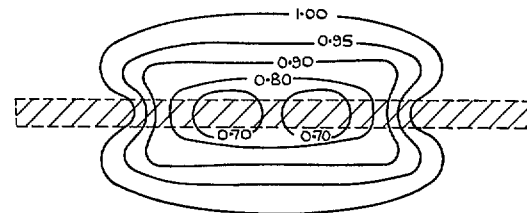
(c) VELOCITY U/U_o

FIGS. 8a to 8c. Flow behind flat plate of aspect ratio 20.—Total head, static pressure and velocity contours behind plate $\left(\frac{x}{\sqrt{S}} = 3.60; \frac{x}{X} = 3.75\right)$.
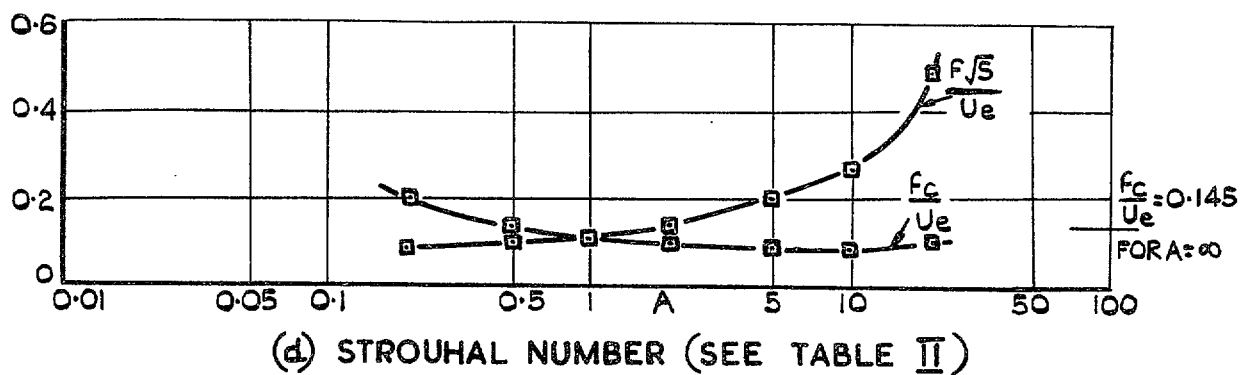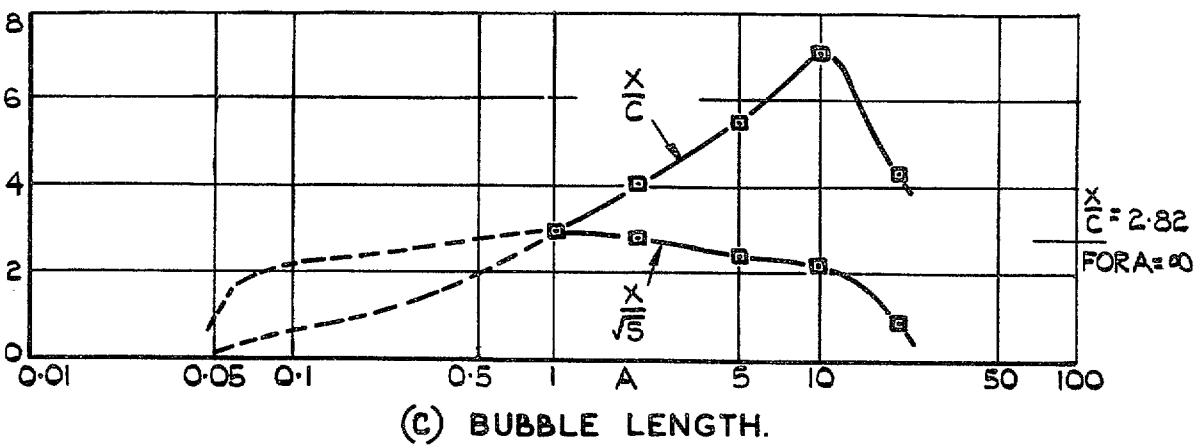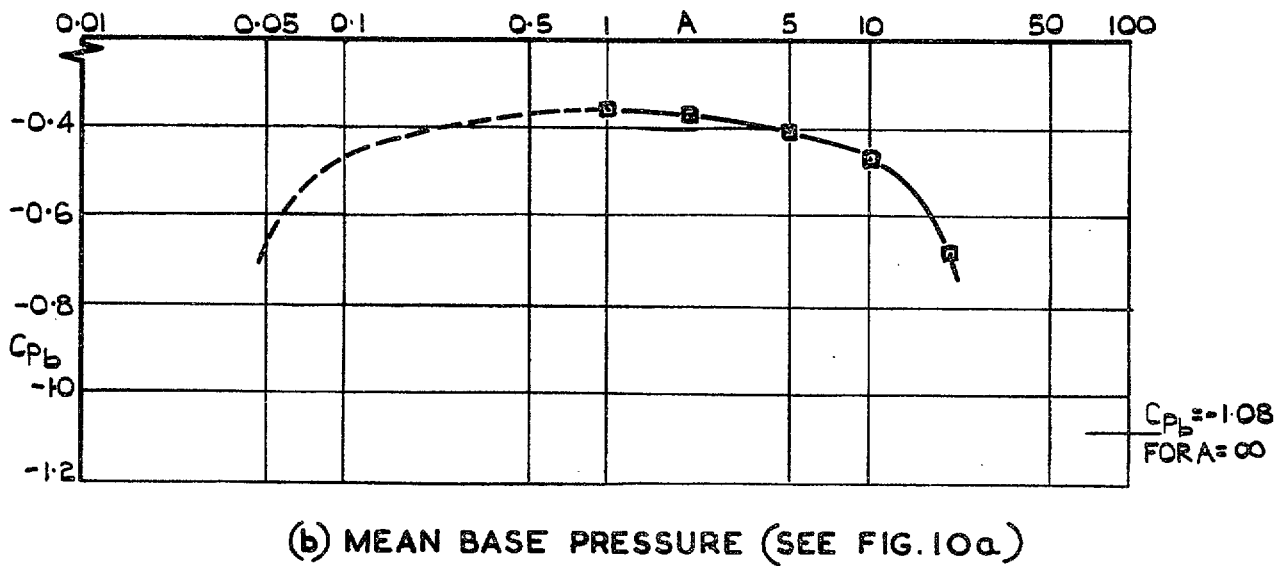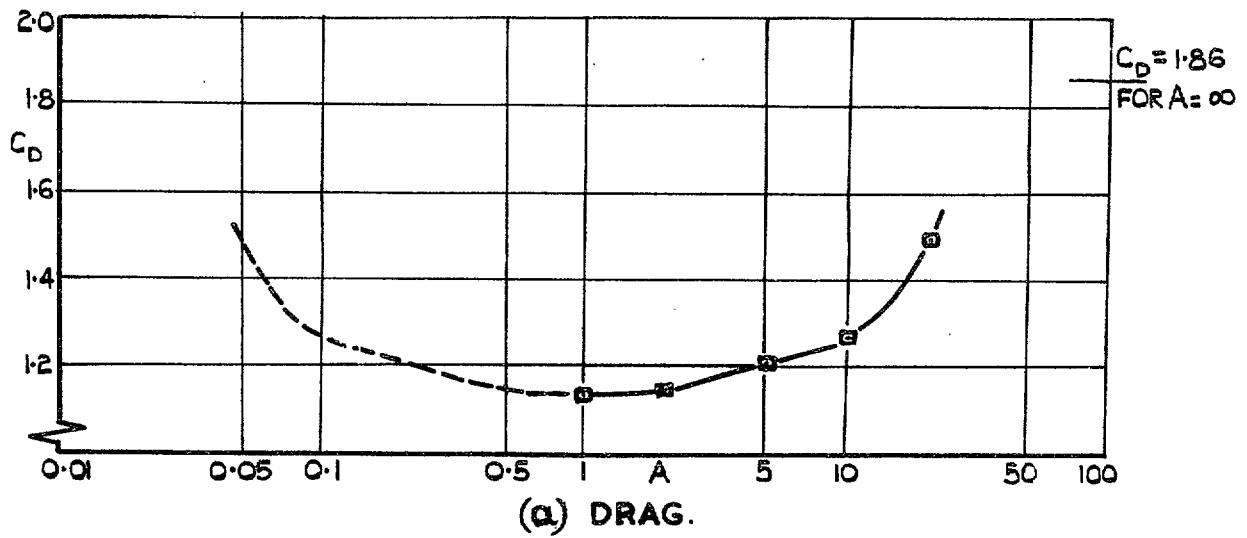
FIGS. 9a to 9d. Rectangular flat plates. — Variation of drag, base pressure, bubble length and Stroubal Number with aspect ratio.
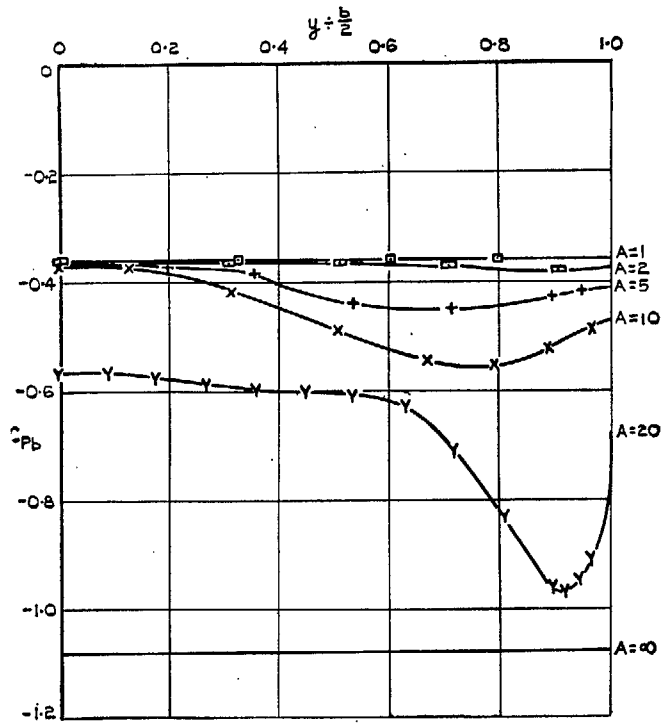
FIG. 10a. Spanwise distribution of static pressure
on rear face (Corrected for tunnel blockage).
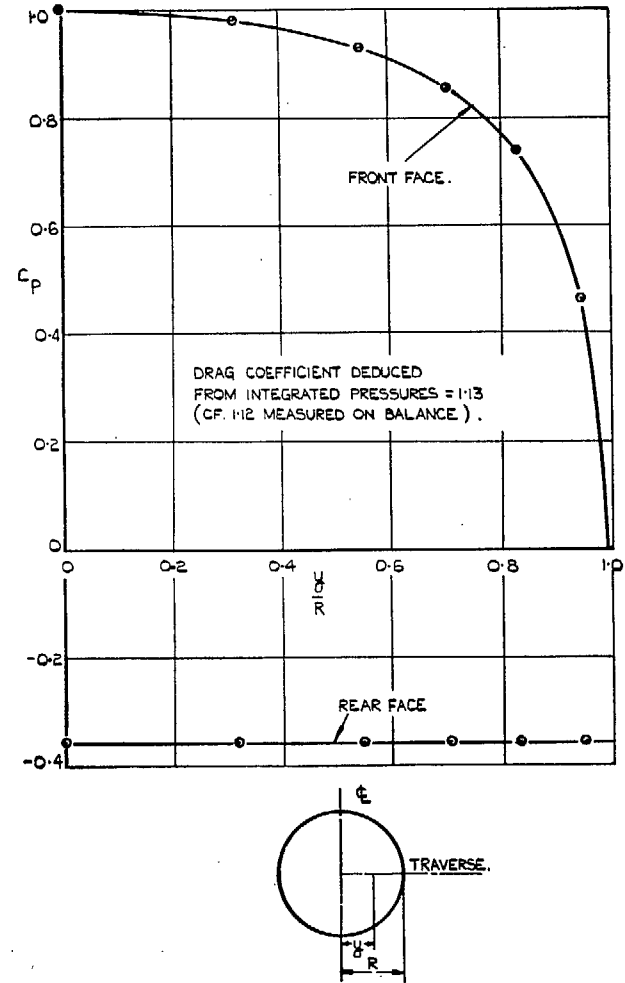
FIG. 10b. Static-pressure distribution on front
and rear faces of circular plate (Corrected for
tunnel blockage).
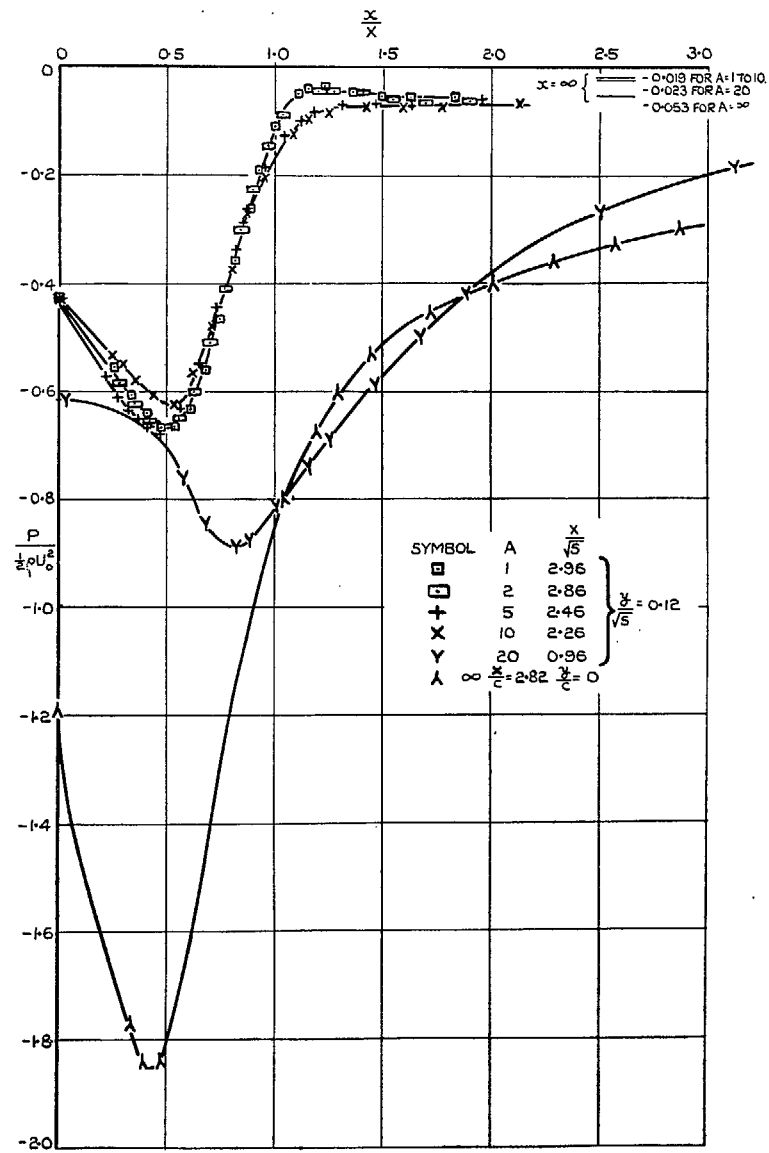
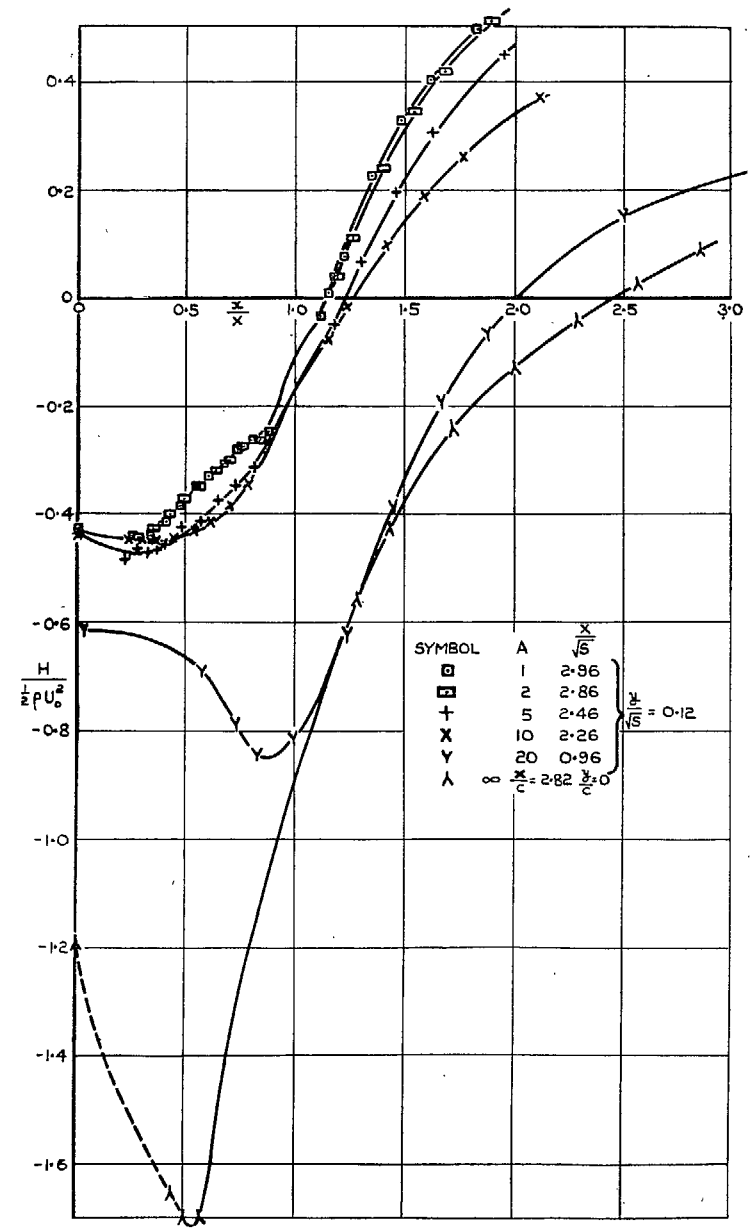FIG. 11a.   Total head near axis of rectangular plates.

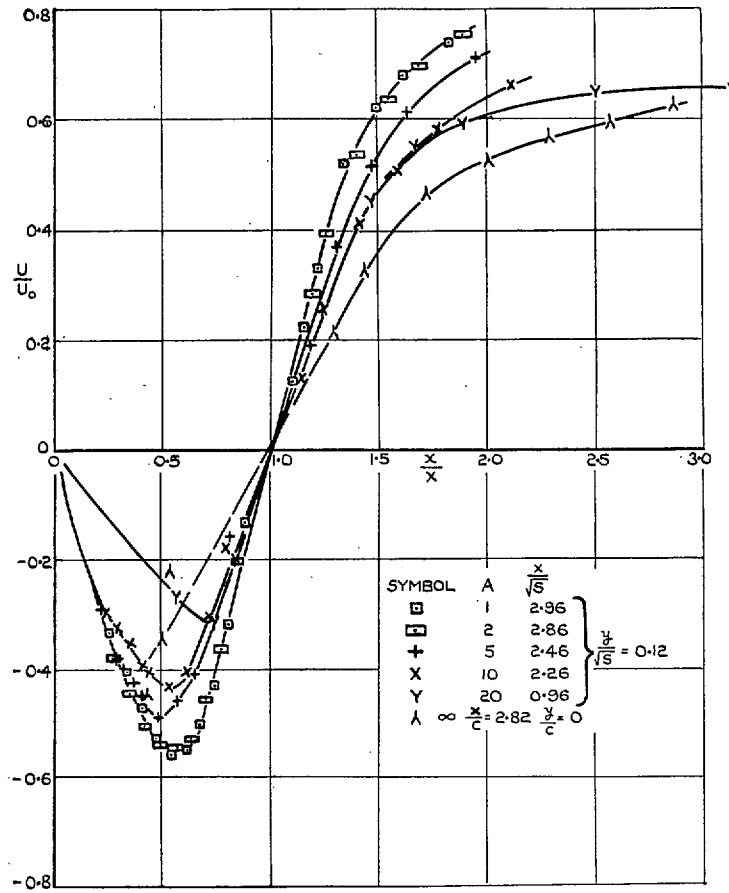FIG. 11b.   Static pressure near axis of rectangular plates.

18

FIG. 11c. Velocity near axis of rectangular plates.
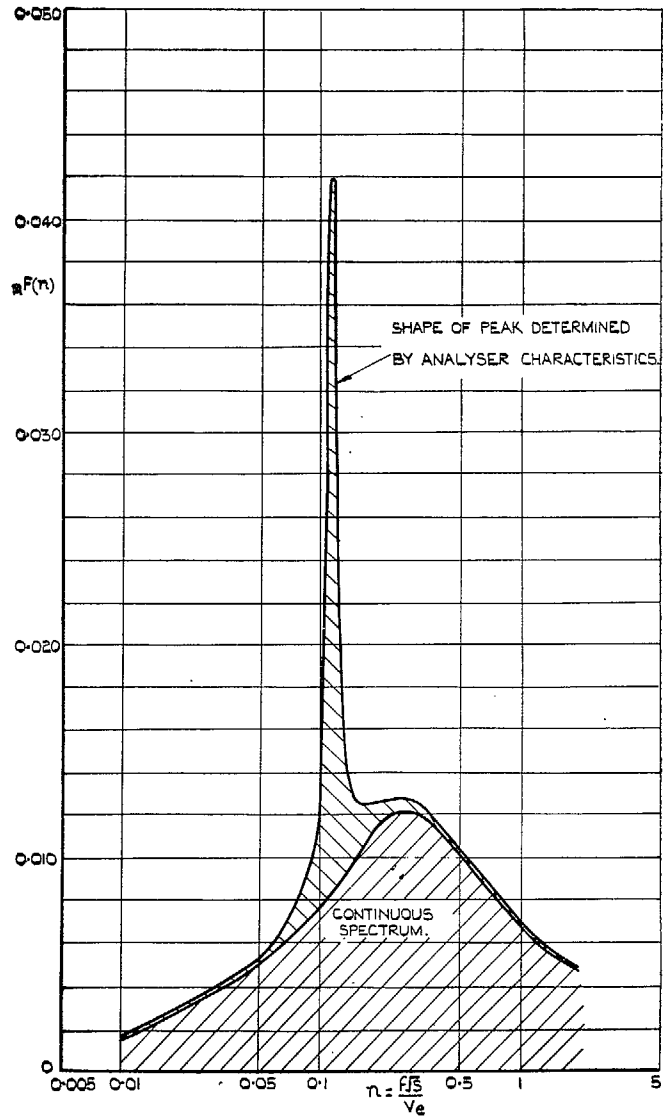
FIG. 12b. Analysis of velocity fluctuations behind square plate $(x/\sqrt{S} = 3\cdot60; y/\sqrt{S} = 0\cdot80)$.
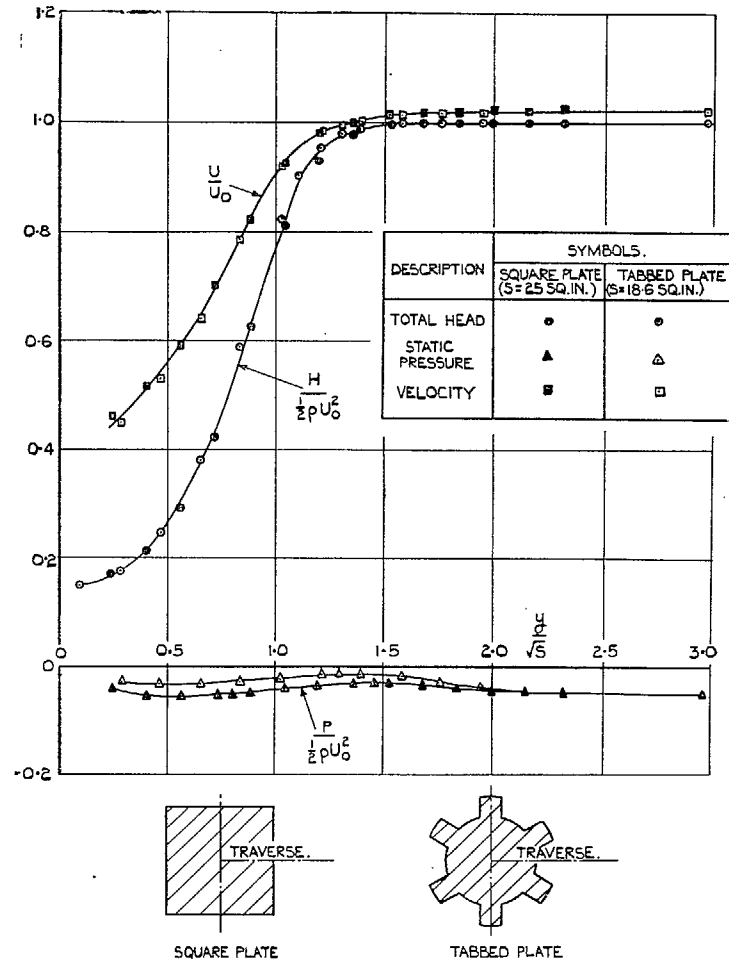
FIG. 13. Comparison of total head, static pressure and velocity distribution behind square plate and tabbed plate $(x/\sqrt{S} = 3\cdot60)$.
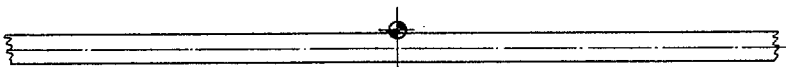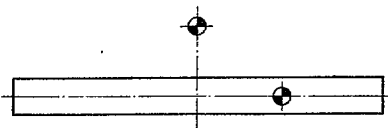
A = ∞, x/χ = 1·285, x/c = 3·63.

NOTE:– SPECTRA OF $\left(u/U_e\right)^2$ MEASURED AT POINTS INDICATED THUS ⊕ WHERE MAX. VALUE OF u/U_e OCCURS.
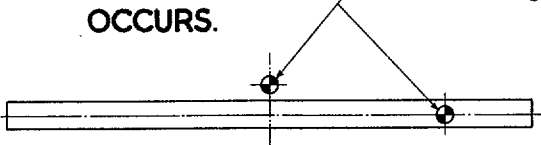
A = 20, x/χ = 1·24, $x/\sqrt{s}$ = 1·19.

A = 10, x/χ = 1·24, $x/\sqrt{s}$ = 2·80.

CHORDWISE TRAVERSE

SPANWISE TRAVERSE

A = 5, x/χ = 1·24, $x/\sqrt{s}$ = 3·06.

A = 2, x/χ = 1·22, $x/\sqrt{s}$ = 3·48.

A = 1, x/χ = 1·22, $x/\sqrt{s}$ = 3·60.

CHORDWISE TRAVERSE

SPANWISE TRAVERSE

u/U_e

y/c

$y/\sqrt{s}$ & $z/\sqrt{s}$

$n F(n)$

$z/c = 0.64$

$n = \frac{fc}{U_e}$

$z/\sqrt{s} = 0.26$ $y/\sqrt{s} = 1.50$

$n = \frac{f\sqrt{s}}{U_e}$

$z/\sqrt{s} = 0.6$ $y/\sqrt{s} = 0.72$

$z/\sqrt{s} = 0.84$ $y/\sqrt{s} = 0.54$

$z/\sqrt{s} = 0.9$ $y/\sqrt{s} = 0.8$

$z/\sqrt{s} = 0.8$
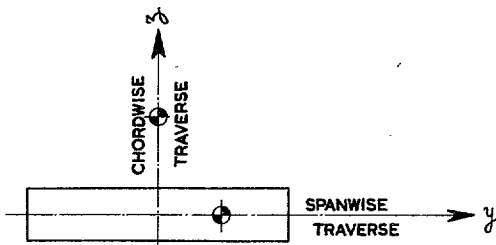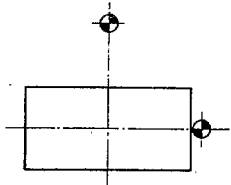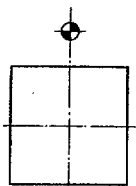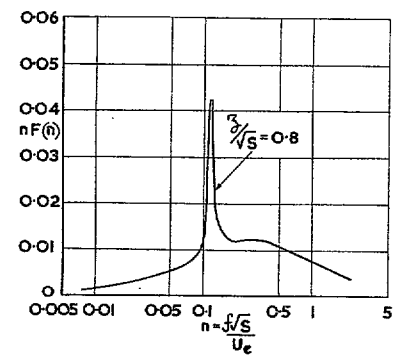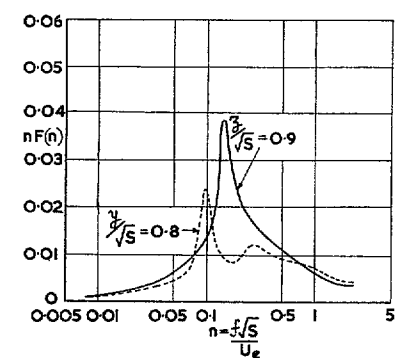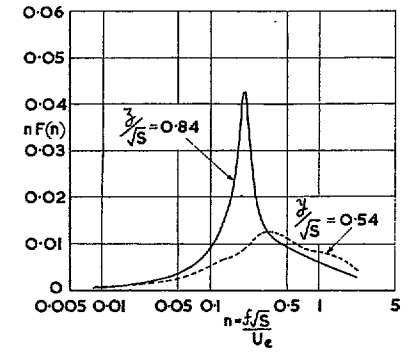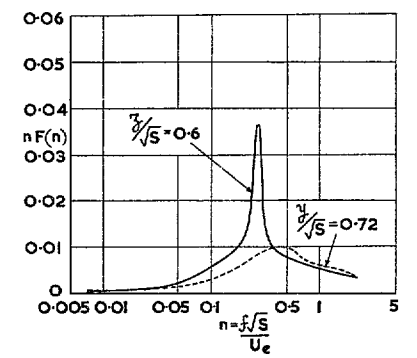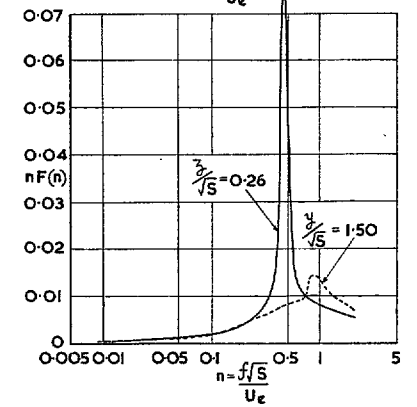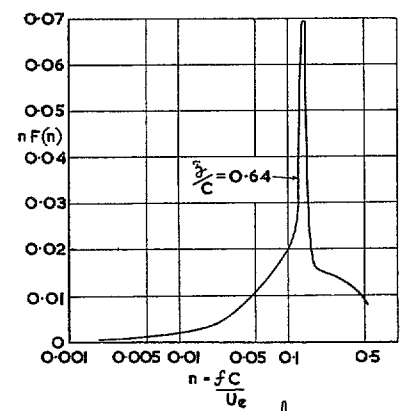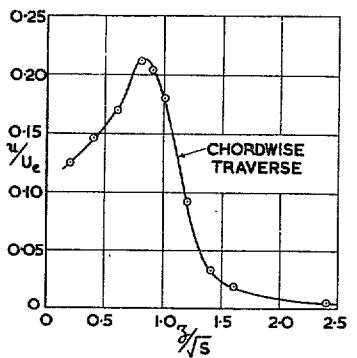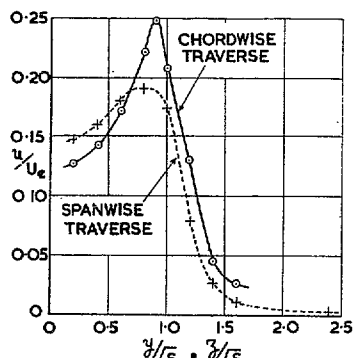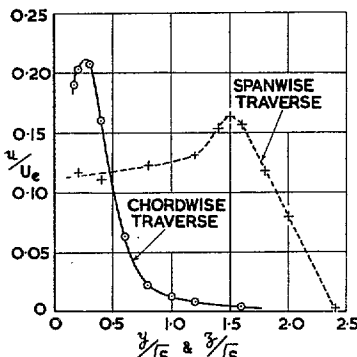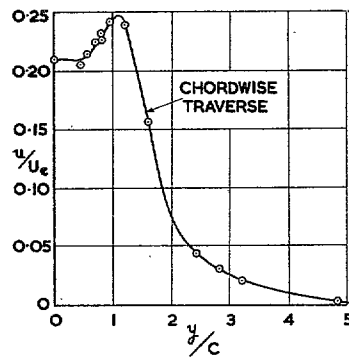
FIG. 12a. Flow behind flat plates. — Measurements of r.m.s. velocity fluctuations and spectra of $(u/U_e)^2$.

FIG. 14. Comparison of total head, static pressure and velocity near axis of square plate and tabbed plate $(y/\sqrt{S} = 0\cdot12)$.
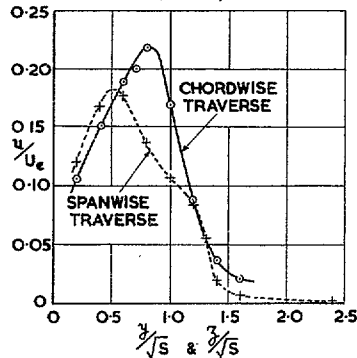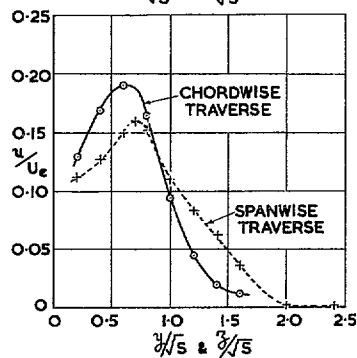
(a) R.M.S. VELOCITY FLUCTUATION.

(b) SPECTRA OF $\left(\dfrac{u}{U_e}\right)^2$

FIGS. 15a and 15b. Comparison of velocity fluctuations behind square, circular and tabbed plates $(x/\sqrt{S} = 3\cdot60; x/X \simeq 1\cdot2)$.

Publications of the Aeronautical Research Council

ANNUAL TECHNICAL REPORTS OF THE AERONAUTICAL RESEARCH COUNCIL (BOUND VOLUMES)

1939 Vol. I. Aerodynamics General, Performance, Airscrews, Engines. 50s. (52s.).
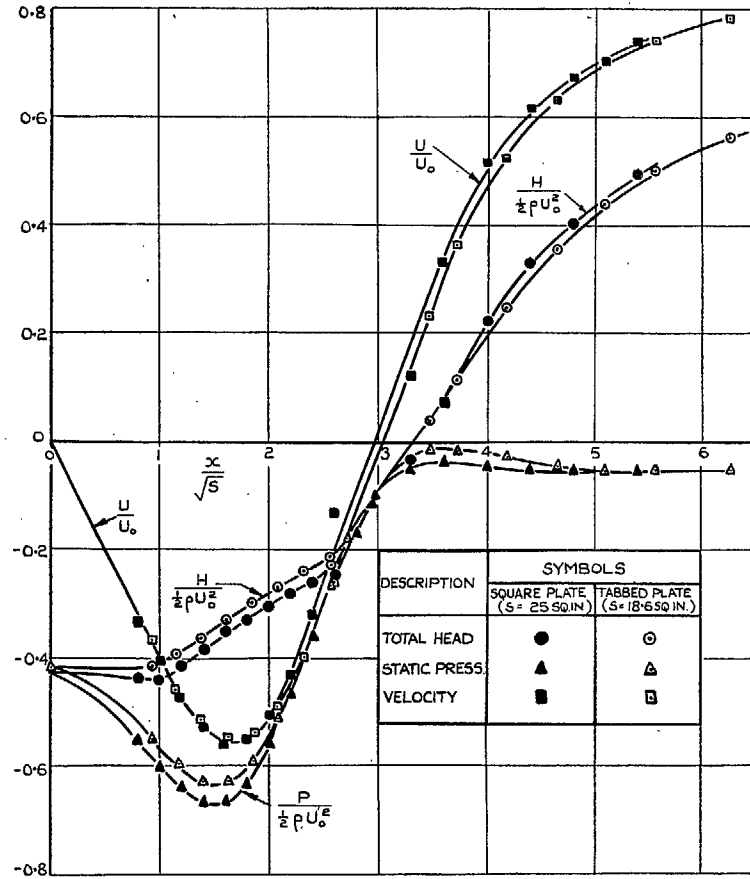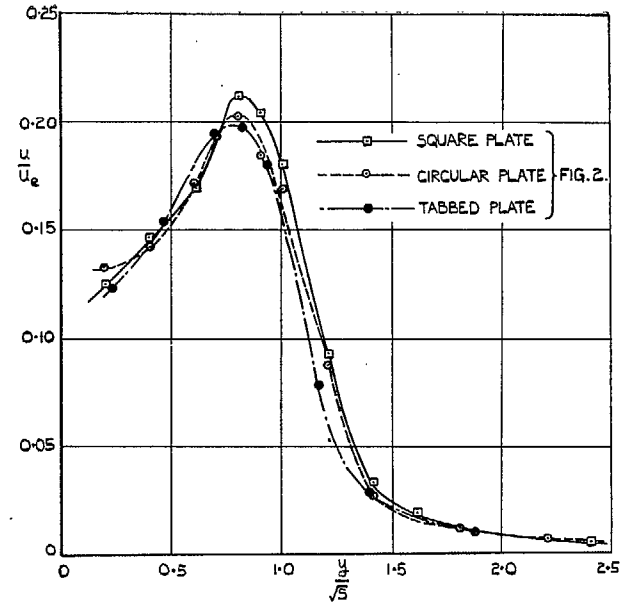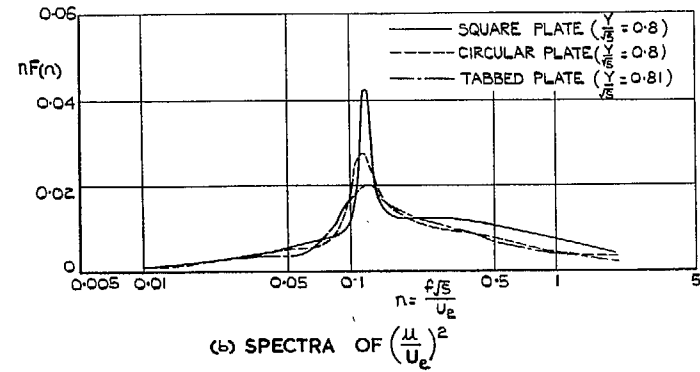Vol. II. Stability and Control, Flutter and Vibration, Instruments, Structures, Seaplanes, etc. 63s. (65s.)

1940 Aero and Hydrodynamics, Aerofoils, Airscrews, Engines, Flutter, Icing, Stability and Control, Structures, and a miscellaneous section. 50s. (52s.)

1941 Aero and Hydrodynamics, Aerofoils, Airscrews, Engines, Flutter, Stability and Control, Structures. 63s. (65s.)

1942 Vol. I. Aero and Hydrodynamics, Aerofoils, Airscrews, Engines. 75s. (77s.)
Vol. II. Noise, Parachutes, Stability and Control, Structures, Vibration, Wind Tunnels. 47s. 6d. (49s. 6d.)

1943 Vol. I. Aerodynamics, Aerofoils, Airscrews. 80s. (82s.)
Vol. II. Engines, Flutter, Materials, Parachutes, Performance, Stability and Control, Structures. 90s. (92s. 9d.)

1944 Vol. I. Aero and Hydrodynamics, Aerofoils, Aircraft, Airscrews, Controls. 84s. (86s. 6d.)
Vol. II. Flutter and Vibration, Materials, Miscellaneous, Navigation, Parachutes, Performance, Plates and Panels, Stability, Structures, Test Equipment, Wind Tunnels. 84s. (86s. 6d.)

1945 Vol. I. Aero and Hydrodynamics, Aerofoils. 130s. (132s. 9d.)
Vol. II. Aircraft, Airscrews, Controls. 130s. (132s. 9d.)
Vol. III. Flutter and Vibration, Instruments, Miscellaneous, Parachutes, Plates and Panels, Propulsion. 130s. (132s. 6d.)
Vol. IV. Stability, Structures, Wind Tunnels, Wind Tunnel Technique. 130s. (132s. 6d.)

Annual Reports of the Aeronautical Research Council—

1937 2s. (2s. 2d.)   1938 1s. 6d. (1s. 8d.)   1939-48 3s. (3s. 5d.)

Index to all Reports and Memoranda published in the Annual Technical Reports, and separately—

April, 1950   -   -   -   -   R. & M. 2600   2s. 6d. (2s. 10d.)

Author Index to all Reports and Memoranda of the Aeronautical Research Council—

1909—January, 1954   R. & M. No. 2570   15s. (15s. 8d.)

Indexes to the Technical Reports of the Aeronautical Research Council—

December 1, 1936—June 30, 1939	R. & M. No. 1850	1s. 3d. (1s. 5d.)
July 1, 1939—June 30, 1945	R. & M. No. 1950	1s. (1s. 2d.)
July 1, 1945—June 30, 1946	R. & M. No. 2050	1s. (1s. 2d.)
July 1, 1946—December 31, 1946	R. & M. No. 2150	1s. 3d. (1s. 5d.)
January 1, 1947—June 30, 1947	R. & M. No. 2250	1s. 3d. (1s. 5d.)

Published Reports and Memoranda of the Aeronautical Research Council—

Between Nos. 2251–2349	R. & M. No. 2350	1s. 9d. (1s. 11d.)
Between Nos. 2351–2449	R. & M. No. 2450	2s. (2s. 2d.)
Between Nos. 2451–2549	R. & M. No. 2550	2s. 6d. (2s. 10d.)
Between Nos. 2551–2649	R. & M. No. 2650	2s. 6d. (2s. 10d.)
Between Nos. 2651–2749	R. & M. No. 2750	2s. 6d. (2s. 10d.)

Prices in brackets include postage

HER MAJESTY'S STATIONERY OFFICE